ELSEVIER

Coordination Chemistry Reviews
167 (1997) 49–94

COORDINATION CHEMISTRY REVIEWS

Solid-state NMR spectroscopy of mercury compounds

Graham A. Bowmaker [a], Robin K. Harris [b,*], Se-Woung Oh [b,1]

[a] *Department of Chemistry, University of Auckland, Private Bag 92019, Auckland, New Zealand*

[b] *Department of Chemistry, Science Laboratories, University of Durham, South Road, Durham, DH1 3LE, UK*

Received 11 February 1997; accepted 8 August 1997

Contents

1. Introduction, and scope of review

Over the last 20 years there has been a considerable increase in the use of heavy-metal nuclei in solution-state NMR spectroscopy applied to inorganic and organometallic chemistry [1–11], and, with the recent developments in high-resolution

* *Corresponding author. Fax: +44 191 386 1127; e-mail: r.k.harris@durham.ac.uk*

[1] Present address: Department of Chemistry, Mokpo National University, Muan 534-729, Chonnam, South Korea.

PII S0010-8545(97)00053-2

NMR techniques for solids [12–21], there has been increasing interest in the solid-state spectra of such nuclei. Until recently, there were very few solid-state NMR studies involving the magnetic mercury nuclei, but in the last few years there has been a significant increase in the number of such investigations, and it seems appropriate at the present time to review the methods available for studying these systems and the results which have been obtained.

Naturally-occurring mercury contains two magnetic isotopes, ^{199}Hg and ^{201}Hg, whose properties are listed in Table 1. Most studies have involved ^{199}Hg, which is the only spin $I=1/2$ isotope of mercury. With a receptivity greater than five times that of ^{13}C, its potential for the characterization of mercury compounds is considerable, and this potential has been realized to some extent through the interpretation of chemical shift and spin–spin coupling data obtained from ^{199}Hg solution-state NMR studies [1,5,8–10]. Also, the relatively high natural abundance of ^{199}Hg allows the observation of spin–spin coupling to other nuclei as satellite peaks in the spectra of the nuclei concerned (e.g. ^{31}P) [23,24]. However, there are a number of difficulties associated with solution-state measurements which limit the usefulness of the data obtained from such studies. Thus, the relatively high lability of the ligands in mercury complexes can result in the observation of fast-exchange spectra involving equilibria between several species in solution [1,5,8–10,25]. Related to this is the fact that the spectra can be very solvent- and/or temperature-dependent, possibly due to the interaction of the compounds concerned with solvent molecules and also to the very large chemical shift range and spin–spin coupling constant values which are characteristic of heavy-metal nuclei [1,5,8–10]. Exchange reactions rarely occur in the solid state, so that the effects of such processes are normally absent in solid-state NMR spectra and so the spectra can be unambiguously associated with a particular species. Thus, by studying complexes of known crystal structure, correlations can be established between the NMR and structural parameters. It should be emphasized, however, that "medium effects" are not entirely removed from the spectra; the existence of molecular interactions in the solid has manifestations in solid-state NMR spectra, but these interactions are much more clearly defined in the solid than in the solution state, so that their effects can be studied in much more detail. As well as providing the same kind of data (isotropic chemical shifts and scalar spin–spin coupling constants) as are available from solution-state studies, solid-state NMR spectroscopy yields additional information (chemical shift anisotropy and asymme-

Table 1
NMR properties of the magnetic isotopes of mercury ([22])

Isotope	Natural abundance	Spin, I	Magnetic moment, μ/μ_N	Magnetogyric ratio, γ (10^7 rad T^{-1} s^{-1})	Quadrupole moment, Q (10^{-28} m^2)	NMR frequency, Ξ (MHz)	Relative receptivity, D^C
^{199}Hg	16.87	1/2	0.87621937	4.8457916	–	17.910323	5.73
^{201}Hg	13.18	3/2	−0.7232483	−1.788769	0.385	6.611400	1.13

try, coupling constant anisotropy, dipolar coupling constants) which can be used to probe the structure and bonding in the molecules concerned.

The normal oxidation state of mercury in its complexes is +2; there are considerably smaller numbers of compounds in lower oxidation states, the main ones involving complexes of the Hg–Hg bonded mercury(I) ion, Hg_2^{2+} [26,27]. The structural chemistry of mercury(II) is characterized by a tendency towards two-coordination, but the presence of secondary bonding interactions often results in an expansion of the mercury coordination sphere to give a higher effective coordination number [26–31]. This results in a rich and varied structural chemistry. In recent years an interest in the interference of mercury with biological systems has provided an additional incentive for a better understanding of mercury coordination chemistry [10]. Spectroscopic methods have played a significant role in the characterization of mercury complexes [31,32], but the closed-shell $5d^{10}$ electron configuration of Hg^{2+} precludes the use of several of the physical methods (e.g. paramagnetism, d–d transition spectra) which are applicable to other transition metal compounds. Thus, the use of NMR spectroscopy involving the magnetic Hg nuclei is particularly attractive as a method for investigating the structure and bonding in mercury compounds. The present review covers studies involving solid-state NMR spectroscopy of mercury compounds, with the restriction that the spectra concerned are dependent on the presence of interactions involving the magnetic nuclei ^{199}Hg or ^{201}Hg in the nuclear spin Hamiltonian. This includes all solid-state ^{199}Hg and ^{201}Hg NMR studies, as well as solid-state NMR spectra of other nuclei where effects of coupling to ^{199}Hg or ^{201}Hg are evident. Previous reviews on the solid-state NMR of metal nuclei have included short sections on solid-state ^{199}Hg NMR spectroscopy [15,16].

2. Theory

2.1. The shielding tensor

In an NMR experiment the field $\boldsymbol{B}$ experienced by a nucleus is related to the applied field $\boldsymbol{B}_0$ by

$$\boldsymbol{B} = \boldsymbol{B}_0(1-\boldsymbol{\sigma}) \tag{1}$$

where $\boldsymbol{\sigma}$ is known as the shielding tensor [19]. It is a second-rank tensor which is determined by the electronic distribution around the nucleus. In general, the magnetic field at the nucleus depends on the orientation of the external magnetic field relative to the relevant molecule or fragment, i.e. the shielding is anisotropic. The principal components σ_{11}, σ_{22}, σ_{33} of the shielding tensor are the diagonal elements of the tensor in the principal axis system (the coordinate system in which all of the off-diagonal elements of the symmetrical part of the tensor are zero). For nuclei which lie on crystallographic symmetry axes or planes, the principal axes lie along the symmetry axes and/or in the symmetry planes; in other cases the locations of these

axes can only be determined by measurement or calculation. A special case concerns a nucleus at a site of axial symmetry, where the nucleus lies on an axis of threefold or higher symmetry. In this case, the following notation is adopted

$$\sigma_{\parallel} = \sigma_{33} \tag{2}$$

$$\sigma_{\perp} = \sigma_{11} = \sigma_{22} \tag{3}$$

The isotropic, or scalar, shielding constant σ_{iso}, is defined as

$$\sigma_{iso} = (1/3)(\sigma_{11} + \sigma_{22} + \sigma_{33}) \tag{4}$$

In order to permit unambiguous definition of the shielding anisotropy and asymmetry (see below) the principal axes are normally assigned according to the convention [22,33,34]

$$|\sigma_{33} - \sigma_{iso}| \geq |\sigma_{11} - \sigma_{iso}| \geq |\sigma_{22} - \sigma_{iso}| \tag{5}$$

Two parameters are in common use in the literature to describe the anisotropy of the shielding tensor. Both are referred to as the "shielding anisotropy", but they have different definitions [33,34]

$$\Delta\sigma = \sigma_{33} - 1/2(\sigma_{11} + \sigma_{22}) \tag{6}$$

$$\zeta = \sigma_{33} - \sigma_{iso} \tag{7}$$

Using Eq. (4), it can be shown that

$$\zeta = (2/3)\Delta\sigma \tag{8}$$

so the two parameters are directly proportional to each other, but care should be taken to specify which of them is being used. In this review, we will use $\Delta\sigma$ exclusively to describe the shielding anisotropy. The departure of the shielding tensor from axial symmetry is described by the asymmetry parameter [33], which is defined as

$$\eta = (\sigma_{22} - \sigma_{11})/(\sigma_{33} - \sigma_{iso}) = (\sigma_{22} - \sigma_{11})/5 \tag{9}$$

With the axis-labelling convention (Eq. (5)), it can be shown that

$$0 \leq \eta \leq 1 \tag{10}$$

with $\eta = 0$ corresponding to the case of axial symmetry ($\boldsymbol{\sigma}_{11} = \boldsymbol{\sigma}_{22}$). While η is always positive according to the above definitions, the anisotropy parameters $\Delta\boldsymbol{\sigma}$ and ζ may be either positive or negative.

The shielding results in a chemical shift of the NMR signal so that it occurs at a frequency ν in the sample compared with a reference signal at ν_r for the same isotope in a reference substance. According to the IUPAC convention [35], the chemical shift relative to the reference is defined as in Eq. (11), but is usually quoted in ppm (so that 10^6 may be incorporated into the definition).

$$\delta = (\nu - \nu_r)/\nu_r \tag{11}$$

The absolute shielding σ which results from the definition in Eq. (1) can be expressed (again usually in ppm) in terms of the resonance frequency ν in the sample and the frequency ν_n of the bare nucleus

$$\sigma = (\nu_n - \nu)/\nu_n \tag{12}$$

The relationship between the shift and the shielding is

$$\delta = (\sigma_r - \sigma)/(1 - \sigma_r) \tag{13}$$

where σ_r is the is the isotropic shielding for the reference substance. Thus

$$\sigma - \sigma_r \approx -\delta \tag{14}$$

if $\sigma_r \ll 1$.

Another quantity which reflects the anisotropy of the chemical shift or shielding tensor has been recently described [33]. This is referred to as the span of the tensor and is defined as

$$\Omega = \sigma_{33} - \sigma_{11} \tag{15}$$

with the principal axes ordered such that

$$\sigma_{11} \leq \sigma_{22} \leq \sigma_{33} \tag{16}$$

(contrast Eq. (5)). The span is thus defined to be positive and is actually the modulus of the difference between the maximum and minimum principal values of the shielding or chemical shift tensors. The skew of the shielding tensor has been proposed as an alternative to the asymmetry parameter [33], and is defined as

$$\kappa = 3(\sigma_{iso} - \sigma_{22})/\Omega \tag{17}$$

with the principal axis labelling system (Eq. (16)). This results in

$$-1 \leq \kappa \leq +1 \tag{18}$$

with $\kappa = \pm 1$ corresponding to the special case of axial symmetry: $\kappa = +1$ corresponds to $\sigma_\parallel > \sigma_\perp$, while $\kappa = -1$ corresponds to $\sigma_\parallel < \sigma_\perp$ [33] – again, no distinction is made between chemical shift and shielding tensors. These two situations $\kappa = \pm 1$ both yield an asymmetry parameter $\eta = 0$, but they are distinguished by the anisotropy parameters $\Delta\sigma$ and ζ, which are +ve and −ve for the cases $\sigma_\parallel > \sigma_\perp$ and $\sigma_\parallel < \sigma_\perp$, respectively. Most of the papers on solid-state ^{199}Hg NMR published to date have used the anisotropy and asymmetry rather than the span and skew parameters, despite the fact that arguments in favour of the latter have been published [33]. Both sets of parameters will be given in the discussion of ^{199}Hg anisotropic shielding parameters in Section 4.1. For Ω and κ we use the definitions of Ref. [33] in spite of our misgivings over the confusion between chemical shift and shielding tensors.

The standard reference sample recommended for ^{199}Hg NMR spectroscopy is dimethylmercury(II), $HgMe_2$. However, this substance is highly toxic (as has recently been tragically highlighted by the death of an American chemist – see Chem. Eng.

News, June 16 1997 p. 12) and its use as a reference in experimental work presents practical difficulties, so that secondary standards have been proposed. Mercury(II) acetate, $\delta(^{199}Hg) = -2497$ ppm [36], was used in many of the earlier measurements, but suffers from the disadvantage that its ^{199}Hg spectrum shows a large chemical shift anisotropy of more than 1700 ppm. The best secondary standard proposed to date appears to be hexakis(dimethylsulphoxide)mercury(II) trifluoromethanesulphonate, $[Hg(dmso)_6][CF_3SO_3]_2$, $\delta(^{199}Hg) = -2313$ ppm [37]. The advantageous NMR properties of this substance for its use as a reference are its small chemical shift anisotropy (due to the high-symmetry octahedral coordination environment) and a high $^1H \rightarrow ^{199}Hg$ polarization transfer efficiency (arising from the presence of short H–Hg distances) [38].

The factors which determine the values of the shielding tensor parameters for heavy nuclei such as ^{199}Hg are in principle the same as those for lighter nuclei. In practice, the relative importance of some of these factors changes on passing from lighter to heavier nuclei [39]. As with most molecular parameters determined in a condensed phase, there will be contributions from intra- and intermolecular interactions. Theoretical models naturally start from a consideration of intramolecular factors. Quantum mechanical calculations of the nuclear shielding tensor are frequently expressed in the formalism first developed by Ramsey [40], which involves a sum of diamagnetic (σ^d) and paramagnetic (σ^p) terms.

$$\sigma = \sigma^d + \sigma^p \tag{19}$$

This was extended by Pople to a form which was more amenable to molecular orbital calculations [41]

$$\sigma = \sigma^d(\text{loc}) + \sigma^d(\text{nonloc}) + \sigma^d(\text{inter}) + \sigma^p(\text{loc}) + \sigma^p(\text{nonloc}) + \sigma^p(\text{inter}) \tag{20}$$

where σ^d(loc), σ^p(loc) arise from electronic currents localized on the atom containing the nucleus of interest, σ^d(nonloc), σ^p(nonloc) are derived from currents on neighbouring atoms, and σ^d(inter), σ^p(inter) are interatomic terms involving currents which are not localized on a single atom, e.g. ring currents. While the non-local and interatomic terms may be important for lighter nuclei, particularly for ^1H, they are normally negligible in the case of heavy nuclei [39]. Molecular orbital expressions for the local shielding terms, σ^d(loc), σ^p(loc), involve a sum over states which, in the case of the paramagnetic term, includes unoccupied as well as occupied states. The terms in the latter case involve $(E_k - E_j)^{-1}$ where j, k refer to occupied and unoccupied states, respectively. Since the excitation energies $E_k - E_j$ are generally unknown, these are frequently replaced by a single average energy difference ΔE in what is known as the average excitation energy (AEE) approximation [39]. This is normally coupled with a restriction of the molecular orbitals considered to those involving the valence p and d orbitals centred on the nucleus of interest, since it is these orbitals which make the greatest contribution to the paramagnetic shielding. Within the AEE approximation, the expressions for the principal components of the local paramagnetic shielding tensor for the case where the shielding is due to

the valence p orbitals only are

$$\sigma^{p}(\mathrm{loc})_{xx} = \sigma_{p}(p_{yy} + p_{zz} - p_{zz}p_{yy} + p_{yz}p_{zy}) \tag{21}$$

$$\sigma^{p}(\mathrm{loc})_{yy} = \sigma_{p}(p_{xx} + p_{zz} - p_{zz}p_{xx} + p_{xz}p_{zx}) \tag{22}$$

$$\sigma^{p}(\mathrm{loc})_{zz} = \sigma_{p}(p_{xx} + p_{yy} - p_{xx}p_{yy} + p_{xy}p_{yx}) \tag{23}$$

where

$$\sigma_{p} = -\mu_{0}e^{2}\hbar^{2}\langle r^{-3}\rangle_{np}/4\pi m^{2}\Delta E \tag{24}$$

and μ_0 is the permeability constant, e is the electronic charge, m is the electron rest mass, $\langle r^{-3}\rangle_{np}$ is the expectation value of r^{-3} for the valence np electron, and the p_{ij} are elements of the charge density/bond order matrix [39,42]. The average, or isotropic, local paramagnetic shielding derived from the above is

$$\sigma^{p}(\mathrm{loc}) = \sigma_{p}(2p_{xx} + 2p_{yy} + 2p_{zz} - p_{zz}p_{yy} - p_{xx}p_{yy} - p_{xx}p_{zz} + p_{yz}p_{zy} + p_{xy}p_{yx} + p_{xz}p_{zx}) \tag{25}$$

For atoms other than hydrogen, differences in the local diamagnetic term caused by changes in chemical bonding are small compared with variations in the local paramagnetic term [42]. Thus, Eqs. (21)–(25) may be used to interpret the shielding parameters for heavier nuclei. Eq. (25) has often been employed to understand trends in isotropic chemical shifts obtained from solution-state NMR spectra of main-group element nuclei (e.g. ^{19}F) [43], where d-orbital involvement in the bonding is unimportant. For the heavier transition metal nuclei, the extended form of this equation involving d orbitals is generally required. However, for Group 12 transition metal compounds which have a closed-shell d^{10} electron configuration, d-orbital involvement in the bonding is expected to be small, and Eq. (25) should be applicable. Thus, trends in the isotropic ^{199}Hg chemical shift in simple mercury(II) compounds were interpreted by use of this equation in some early studies [1], though recent reviews have concentrated more on empirical approaches which have been developed to correlate the large body of chemical shift data with structure and bonding [5,8–10]. Much of the information about the electron distribution which is contained in Eqs. (21)–(23) is lost when the averaged form, Eq. (25), is used but this has been common hitherto because, by and large, only the isotropic shifts have been available. Since solid-state studies often yield the anisotropic shielding parameters as well, and since there has recently been a considerable increase in the amount of data on ^{199}Hg from such studies, it should now be possible to interpret these in terms of Eqs. (21)–(23). It is somewhat surprising to find that there have been few attempts to do this to date, and this question will be examined in more detail in Section 4.1. Mercury compounds are particularly suitable for such an analysis. The simplification which results from the non-involvement of the 5d orbitals in the bonding has already been mentioned above. In addition to this, mercury complexes display a range of different coordination geometries (linear two-coordinate, trigonal three-coordinate, tetrahedral four-coordinate) each of which has a different set of

values for the orbital charge densities and bond orders. This should result in wide variations in the shielding tensor components with changes in the geometry of the complexes. This contrasts with the situation for cadmium complexes, for example, where two-coordination does not occur and three-coordination is rare.

The above analysis involves a number of approximations, and it is semi-empirical because it involves quantities such as σ_p which are normally not evaluated when the method is used to analyse shielding data. At a more fundamental level, such data could be used to test ab initio quantum mechanical calculations. Recent advances in quantum chemical methodology have allowed the development of procedures for the calculation of shielding constants. However, very few results have been reported to date for heavy-metal nuclei. One recent study described the calculation of the ^{199}Hg shielding constants in HgX_2 (X=Cl, Br, I) [44]. This emphasized the importance of including relativistic effects in the calculation; without these, the experimental trends cannot be explained even qualitatively. However, only the isotropic shielding constants were reported in that work. The calculation of the anisotropic ^{199}Hg shielding constants in a mercury compound by ab initio methods is a challenge which has yet to be taken up by theoreticians. Nevertheless, one of the results found in the calculation of the isotropic shielding constants in HgX_2 is relevant to the application of Eqs. (21)–(23); the main source of the large variation in the ^{199}Hg shielding with change in the halogen X is the Fermi-contact term. This is a diamagnetic shielding term which is neglected in the above equations but, since it is isotropic, it does not affect the values of the shielding anisotropy or asymmetry parameters.

2.2. Dipolar coupling

Dipolar coupling between two nuclei A and X is the direct, through-space interaction between the magnetic moments of the nuclei and is represented in the spin Hamiltonian by a tensor $\boldsymbol{D}$, which can be expressed in terms of the dipolar coupling constant

$$D=(\mu_0/4\pi)\gamma_A\gamma_X(\hbar/2\pi)/r_{AX}^3 \tag{26}$$

where γ_A, γ_X are the magnetogyric ratios of the A and X nuclei, and r_{AX} is the distance between the nuclei. The dipolar interaction averages to zero in the solution state, but it results in severe line-broadening in the solid state due to the combined effects of dipolar splitting of the signal under observation caused by interactions with the many neighbouring magnetic nuclei in the solid. This broadening is eliminated in high-resolution solid-state NMR by a combination of techniques (high-power decoupling, magic-angle spinning (MAS), magnetic dilution) [14]. However, if the MAS rate is inadequate, spinning sidebands are seen to an extent which is dependent on the magnitude of the dipolar interaction (when not specifically decoupled). In the presence of other interactions (indirect spin–spin coupling and shielding anisotropy) these sidebands become accentuated and may be analysed to yield data on the interactions in question separately (see Sections 3.4 and 4.3). Also, the presence of strong quadrupole coupling for nuclei dipolar-coupled to the observed

nucleus will cause splittings and line-broadening in the centreband transitions even for fast MAS, which depend on both dipolar and quadrupolar coupling constants (see Sections 2.4 and 4.3).

2.3. Indirect spin–spin coupling

Indirect nuclear spin–spin coupling, as opposed to direct or dipolar spin–spin coupling, is an intramolecular interaction between nuclear spins which is conveyed by the electrons in the molecule. It is well known that such interactions can be mediated by three distinct mechanisms; namely, the Fermi-contact, spin–orbital and spin–dipolar mechanisms [45–47]. The indirect spin–spin coupling interaction is in general anisotropic, and is represented by a tensor ***J***. Solution studies yield the average (or isotropic) value, which is the trace of the ***J*** tensor. High-resolution solid-state NMR spectroscopy offers the opportunity to measure the anisotropy of the ***J*** tensor (though any asymmetry is usually ignored). Since the Fermi-contact interaction is purely isotropic [45], the anisotropy in ***J*** gives direct evidence concerning the existence of non-Fermi contact interactions. Examples of such studies involving $^1J(^{199}\mathrm{Hg},^{31}\mathrm{P})$ coupling will be discussed in Section 4.3. Due to the low receptivity of ^{199}Hg relative to ^{31}P, and the large shielding anisotropy affecting ^{199}Hg spectra, the measurements are normally made by using the ^{199}Hg satellites in the spectra of the more abundant ^{31}P nucleus.

2.4. Nuclear quadrupole coupling

Nuclear quadrupole coupling involves the interaction of the electric quadrupole moment of the nucleus with the electric field gradient at the nucleus. The electric field gradient arises from the distribution of electric charges (electrons, neighbouring nuclei) about the nucleus in question, and is represented by the tensor quantity ***eq*** ($eq_{ij}=\partial^2 V/\partial x_i \partial x_j$, where V is the electric potential at the nucleus, x_i, $x_j = x, y, z$). The principal axes of this tensor are often defined such that

$$|eq_{zz}| \geq |eq_{yy}| \geq |eq_{xx}| \tag{27}$$

which is not consistent with convention (Eq. (5)) for the shielding tensor. Since the electric field gradient tensor is traceless ($eq_{xx}+eq_{yy}+eq_{zz}=0$), it can be represented by just two parameters, the "principal component" of the electric field gradient

$$eq = eq_{zz} \tag{28}$$

and the field-gradient asymmetry parameter

$$\eta = (eq_{xx} - eq_{yy})/eq_{zz} \tag{29}$$

Unfortunately, the symbol normally used for this latter quantity is the same as that used for the shielding tensor asymmetry parameter, Eq. (9). The nuclear quadrupole coupling constant $\chi = e^2qQ/h$ (in frequency units) is proportional to the product of the electric field gradient parameter eq with the nuclear quadrupole moment eQ.

The field gradient tensor eq is strongly dependent on the coordination environment of the nucleus involved; perfect tetrahedral coordination results in $eq=0$, but linear two-coordination and trigonal three-coordination yield non-zero eq.

Of the two magnetic isotopes of mercury, only ^{201}Hg possesses a quadrupole moment (Table 1). The value of the quadrupole moment is quite high and this, coupled with the fact that mercury compounds often have structures in which the mercury coordination number is low, means that ^{201}Hg quadrupole coupling constants are generally large in magnitude. Nuclear quadrupole coupling constants can be measured by a variety of methods [48], but for solid samples involving large quadrupole coupling constants, nuclear quadrupole resonance (NQR) spectroscopy is still the best method. This involves the direct measurement of transitions between the nuclear spin states which are split by the quadrupole interaction (in the absence of an applied magnetic field). In the case of ^{201}Hg, which has spin $I=3/2$, the quadrupole interaction produces a separation of the $\pm 1/2$ and $\pm 3/2$ spin states, and the frequency of the transition between these is

$$\nu(\pm 1/2 \leftrightarrow \pm 3/2)=(\chi/2)(1+\eta^2/3)^{1/2} \tag{30}$$

Very few ^{201}Hg NQR studies have reported to date. In one such study, the ^{201}Hg frequencies for $HgCl_2$ and the dioxan solvates HgX_2.2dioxan (X=Cl, Br) were measured, yielding the values 354.21, 323.38 and 313.23 MHz, respectively [49]. That report provides an estimate of the ^{201}Hg quadrupole coupling constants in these compounds. The HgX_2 molecules in the compounds concerned have an essentially linear, two-coordinate geometry for which the field gradient asymmetry parameter $\eta \approx 0$. Thus, from Eq. (30), the coupling constants χ are approximately twice the resonance frequencies, and so are in the vicinity of 700 MHz.

The decrease in the ^{201}Hg NQR frequency from $HgCl_2$ to its solvate has been interpreted in terms of an increase in the ionic character of the Hg–Cl bond, and this was supported by the observation of a corresponding decrease in the ^{35}Cl NQR frequency. The decrease in the ^{201}Hg frequency from the X=Cl to the X=Br solvate was found to be more difficult to explain. An increase was expected on the basis of a bonding scheme involving sp hybridization on the mercury atom, assuming that bromide would be a stronger electron donor than chloride [49]. However, the situation is analogous to that found for the ^{197}Au quadrupole coupling constants in the complexes $[AuX_2]^-$, which are isoelectronic with HgX_2, and the explanation of the observed trend is likely to be the same in both cases, namely an expansion of the $6p_z$ orbital in the bromo- relative to the chloro-complex [50]. The effect of this expansion is to reduce the field gradient produced by electron density in the $6p_z$ orbital, and this opposes the effect of the increased charge transfer to this orbital from bromide relative to chloride, so that the coupling constants for the two compounds are very similar.

The large magnitude of ^{201}Hg quadrupole coupling constants is the main reason why the ^{201}Hg nucleus is generally unsuitable for NMR studies. A large value for the nuclear quadrupole coupling constant frequently results in an efficient relaxation mechanism which in turn causes severe broadening of the NMR transitions. Only

one solid-state ^{201}Hg NMR study of a mercury compound has been reported to date, involving the complex $K_2[Hg(CN)_4]$. In this compound, the mercury lies on a site of tetrahedral symmetry, so that the electric field gradient (and thus the ^{201}Hg quadrupole coupling constant) is in principle zero. The ^{201}Hg signal was observed using several magnetic field strengths, and showed linewidths which were three to four times greater than those of the corresponding ^{199}Hg signals [51]. This increase in linewidth is probably due to the fact that asymmetric vibrations of the molecule cause an effective lowering of symmetry, so that the mercury atom no longer occupies a site of perfect T_d symmetry, and the field gradient is non-zero. This affects the ^{201}Hg nucleus by introducing a non-zero nuclear quadrupole coupling, but not the ^{199}Hg nucleus, which has no quadrupole moment.

The large magnitude of ^{201}Hg quadrupole coupling constants should also lead to the elimination of splittings due to spin–spin couplings involving the ^{201}Hg nucleus, since rapid transitions between the ^{201}Hg spin states which are induced by quadrupolar relaxation result in an averaging of the coupling interaction to zero. This is found to be the case in most NMR studies of mercury complexes. In fact, the compound $K_2[Hg(CN)_4]$, in which the mercury atom lies on a site of cubic symmetry, shows no sign of isotropic $^1J(^{201}Hg,^{13}C)$ coupling in its solid-state ^{13}C NMR spectrum [52], despite the fact that the ^{201}Hg quadrupole coupling constant is sufficiently small to allow direct observation of a ^{201}Hg NMR signal, as discussed above [51]. However, satellites which have been attributed to isotropic $^1J(^{201}Hg,^{31}P)$ coupling have been observed in the solid-state ^{31}P spectra of the complexes $[Hg(PPh_3)X]^+$ (X = Cl, Br, I) [53,54], and these are discussed in more detail in Section 4.2. The observation of coupling in such cases, which involves near-linear coordination of mercury, is unexpected, since the associated large ^{201}Hg quadrupole coupling would normally result in elimination of the spin–spin splitting. Clearly there are factors involved in the coupling of ^{201}Hg to spin-1/2 nuclei which require further clarification.

3. Experimental methods and spectral analysis

3.1. Static measurements

High-resolution solid-state NMR spectra of mercury complexes have generally been carried out by using the technique of magic-angle spinning to improve the sensitivity of detection and the resolution of the spectra (Section 3.2). However, spectra of static samples have been reported in several cases. These studies can be divided into two classes; those involving single crystals, and those using polycrystalline (or powder) samples.

Single-crystal studies are carried out very rarely, due partly to the problems involved in obtaining single crystals of sufficiently large size to produce detectable NMR signals. However, if this problem can be overcome, there are distinct advantages in using single crystals. The first of these is that in some cases the principal axes of the nuclear shielding tensor for all corresponding nuclei in the sample have

the same orientation relative to the external magnetic field direction (e.g. for low-symmetry space groups), so that all of the intensity of the signal occurs essentially at a single chemical shift for a given orientation of the crystal in the magnetic field, rather than being spread over the whole range corresponding to the span of the shielding tensor. The second advantage is that the directions of the principal axis system relative to the molecule can be determined if the crystal structure of the compound concerned is known.

The only mercury complex for which a single-crystal ^{199}Hg NMR study has been reported is, to our knowledge, the dimercury(I) compound $Hg_2(NO_3)_2.2H_2O$ [55]. This compound contains almost linear $[H_2O–Hg–Hg–OH_2]^{2+}$ species (Hg–Hg–O = 167.5°), and the shielding tensor was found to be almost axially symmetric, with the unique element σ_{33} approximately parallel to the long axis of this ion, but lying closer to the Hg–O direction than to the Hg–Hg direction.

Single-crystal ^{31}P NMR studies of some mercury(II) complexes containing tertiary phosphine ligands have been reported [56,57]. The aim of these studies has been to measure the anisotropy of the indirect $^1J(^{199}Hg,^{31}P)$ coupling, as discussed in Section 2.2. Single-crystal methods are used in this case because the analysis of the coupling data is completely independent of the chemical shift interaction, unlike the situation for powder samples [56].

More frequently, however, static measurements are carried out on powder samples. In this case the sample contains crystallites whose principal axes are randomly distributed relative to the external magnetic field direction, and this results in a "powder pattern". The forms of these powder patterns for the cases of axial and non-axial (or rhombic) symmetry are well known [13,14,19]. The main disadvantages of this method in ^{199}Hg NMR studies are that: (i) the chemical shift anisotropy is often very large, so the spectrum is spread over a very wide frequency range, with a consequent loss in sensitivity; and (ii) dipolar or indirect coupling interactions (other than those specifically decoupled) cause further broadening of the resonance band. As an example of a spectrum of a static powder sample, the ^{199}Hg spectrum of $Hg(OAc)_2$ is shown in Fig. 1. This clearly shows that the shielding is not exactly axially symmetric, despite the fact that analysis of the magic-angle spinning spectrum yields $\eta = 0$ under some conditions [36].

3.2. *Magic-angle spinning*

Magic-angle spinning (MAS) involves rotation of the sample about an axis inclined at the magic-angle ($\theta_m = 54.74°$) with respect to the direction of the external magnetic field $\boldsymbol{B}_0$. This method is commonly used in solid-state NMR spectroscopy to remove the line-broadening which is caused by anisotropic interactions such as shielding or heteronuclear dipolar coupling [12–20]. In the extreme case where the spinning speed is much greater than the width of the spectrum due to the anisotropy, MAS yields a single line at the isotropic shift for a single type of nuclear site, but all information about the anisotropy is lost. However, if the spinning frequency is less than the anisotropic spectral width, sidebands form around the isotropic peak at intervals of the spinning frequency. This is often the case for ^{199}Hg MAS NMR

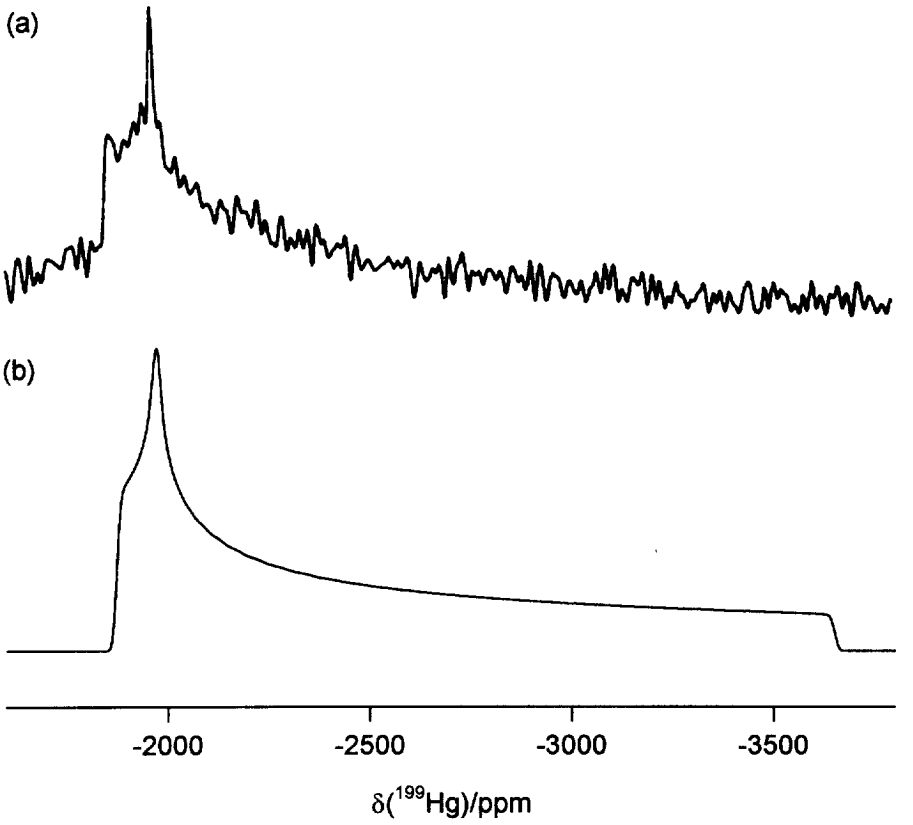

Fig. 1. 53.8 MHz ^{199}Hg spectra of static mercury(II) acetate. (a) Experimental spectrum, cross polarization with spin-echo, 20 ms contact time, 10 s recycle delay, 3470 transients. (b) Computed spectrum, using $\sigma_{11}=1870$, $\sigma_{22}=1968$, $\sigma_{33}=3651$ ppm, $\Delta\nu_{1/2}=1$ kHz. [reproduced, with permission, from Ref. [36]].

spectra, since the chemical shift anisotropy is frequently so large that it is impossible to spin the sample sufficiently rapidly to remove it completely. This results in an effective reduction in sensitivity, since the intensity of the signal is distributed among many peaks in the spectrum. This is one factor which results in the sensitivity of detection for ^{199}Hg NMR spectra often being less than that of ^{13}C, despite the fact that the receptivity of ^{199}Hg is more than five times greater (Table 1). It has been suggested that it is advantageous to obtain ^{199}Hg spectra at low external magnetic field strength, since the frequency width of the spectrum for a given chemical shift anisotropy and asymmetry, and hence the number of observed sidebands, is directly proportional to B_0 [58]. However, the signal intensity is also proportional to the population difference Δn_0 between the α and β spin states of the nucleus, which is in turn proportional to B_0 [14]

$$\Delta n_0 = n_\alpha - n_\beta = N\gamma\hbar B_0/2kT \tag{31}$$

and to other factors dependent on B_0, thus substantially reducing (or perhaps even eliminating) the advantage of using lower field strengths.

The importance of the accurate setting of the angle in MAS NMR spectroscopy has been clearly demonstrated in ^{199}Hg studies. The earliest published high-resolution solid-state ^{199}Hg spectrum was that of mercury(II) acetate, and this exhibited an extensive spinning sideband pattern in which each line showed a small doublet splitting [59]. This splitting was initially attributed to site inequivalence or disorder in the solid [15,59], but it was subsequently shown to be an artefact caused by a deviation of the spinning axis from the magic-angle, which easily happened with the Andrew–Beams design of rotor [36,60]. With the more accurate angle-setting capabilities of modern spectrometers, this is unlikely to be a common problem in future work, but the above studies have clearly established the importance of accurate angle setting (to at least $\pm 0.1°$) in MAS experiments [36].

3.3. Cross polarization

Cross polarization (CP) has been used in combination with magic-angle spinning (MAS) in many ^{199}Hg NMR studies. CP involves the transfer of polarization from an abundant spin system (usually ^{1}H) to a dilute spin system (e.g. ^{199}Hg), and this in principle produces a substantial increase in sensitivity relative to the direct polarization (single-pulse Bloch decay) experiment, primarily for the following two reasons. First, the high proton gyromagnetic ratio (γ_H) leads to a large polarization of the proton spins (H) which can be transferred to the metal nuclei (X) by simultaneous radiofrequency irradiation at the two resonance frequencies for a suitable contact time. This normally requires that the radiofrequency magnetic field amplitudes B_{1H} and B_{1X} are adjusted experimentally to satisfy the Hartmann–Hahn matching condition

$$\omega_{1H} \equiv \gamma_H B_{1H} = \gamma_X B_{1X} \equiv \omega_{1X} \tag{32}$$

This results in equal precession frequencies for H and X ($\omega_{1H} = \omega_{1X}$) about $\boldsymbol{B}_1$ in their respective rotating reference frames, and allows polarization transfer from the protons to the metal nuclei. The maximum theoretical increase in the signal intensity is $\gamma_H/\gamma_X = 4.85$ for X = ^{199}Hg. Second, CP permits a shorter recycle delay and therefore more rapid data acquisition. In the direct polarization method, the recycle delay is determined by the spin-lattice relaxation time T_1 of the metal nucleus X, which can be very long in the solid state. In the CP method, the recycle time is determined by the proton T_1, which is invariably shorter than that of metal nuclei in solids.

Unfortunately, the combination of CP and high-speed MAS has a drawback which severely hinders the study of metal nuclei. Under high-speed MAS conditions, the CP efficiency is low and it is difficult to establish and maintain the exact Hartmann–Hahn match. The CP efficiency at different matching conditions can be presented as a plot of signal intensity versus $\Delta\omega_1$, the difference between the H and X spin-lock frequencies.

$$\Delta\omega_1 = \omega_{1X} - \omega_{1H} \tag{33}$$

Such a plot is referred to as a Hartmann–Hahn matching profile. At low MAS frequencies ω_R, the profile exhibits a broad plateau due to strong proton dipolar couplings, and the maximum signal is relatively insensitive to the matching condition. However, when ω_R becomes comparable to the H–H dipolar couplings, the matching profile is modulated by ω_R and is broken up into a series of sharp peaks with maxima at $\Delta\omega_1 = n\omega_R$, where $n = 0, \pm 1, \pm 2$, etc. [61]. This results in a situation where the maximum signal is very sensitive to the matching condition, and a small mismatch of only a few kilohertz can result in complete loss of signal. Variable-amplitude cross polarization (VACP) is one method which has been proposed to overcome this problem [62]. In this method the amplitude B_1 is varied linearly (or stepwise) with time during the contact period [63], generating multiple matching conditions (each one displaced relative to the others along $\Delta\omega_1$) within a single acquisition. This results in the reduction or removal of the oscillations in the matching profile, so that matching becomes far less critical. The total signal intensity is then comparable to that obtained at low spinning rates, but it is concentrated in fewer spinning sidebands in the spectrum. A study of the application of this method to the heavy-metal nuclei ^{113}Cd and ^{199}Hg has recently been reported [64]. The problems associated with the normal CP MAS method are well illustrated by the ^{199}Hg spectra of $[NMe_4][Hg(S^iPr)_3]$. The spectra at spinning rates of 4, 8 and 12 kHz are shown in Fig. 2. The S/N ratio decreases with increasing spinning rate, despite the improved averaging of the chemical shift anisotropy. The Hartmann–Hahn matching curves for this compound show that for exact matching ($\Delta\omega_1 = 0$), under the conditions used, the total signal for the 12 kHz spinning rate is only one third of that for the 4 kHz rate; a clear demonstration of the limitations of single-amplitude CP MAS discussed above. The curves also show a decrease in the total signal intensity with decreasing $\Delta\omega_1$. As a consequence of this, the most favourable match occurs at $\Delta\omega_1 = \omega_R$ rather than at $\Delta\omega_1 = 0$, and it is suggested that for ^{199}Hg NMR, the matching condition should be centred in the vicinity of $+\omega_R$. A discussion of the factors which determine the optimum values of the other variables in the VACP experiment is given, and it is suggested that for a system whose spectrum has not previously been recorded, values of these parameters may be chosen on the basis of experience with related compounds [64]. However, it is not yet clear to what extent the optimum experimental conditions vary from one compound to another and, from a practical viewpoint, it may be better to obtain the spectra by using direct polarization, with the acquisition of a large number of transients to increase the S/N ratio, rather than by spending a lot of time optimizing the parameters for a CP experiment. This approach also eliminates uncertainties in the analysis of the spectra which arise from possible effects of CP on the intensities of the spinning sidebands though it introduces other problems (see Section 3.4).

3.4. Spinning sideband analysis

While the presence of spinning sidebands due to chemical shift anisotropy usually results in a reduction in the sensitivity of detection of the individual signals in the spectrum, it does allow measurement of the anisotropy parameters, since the intensity

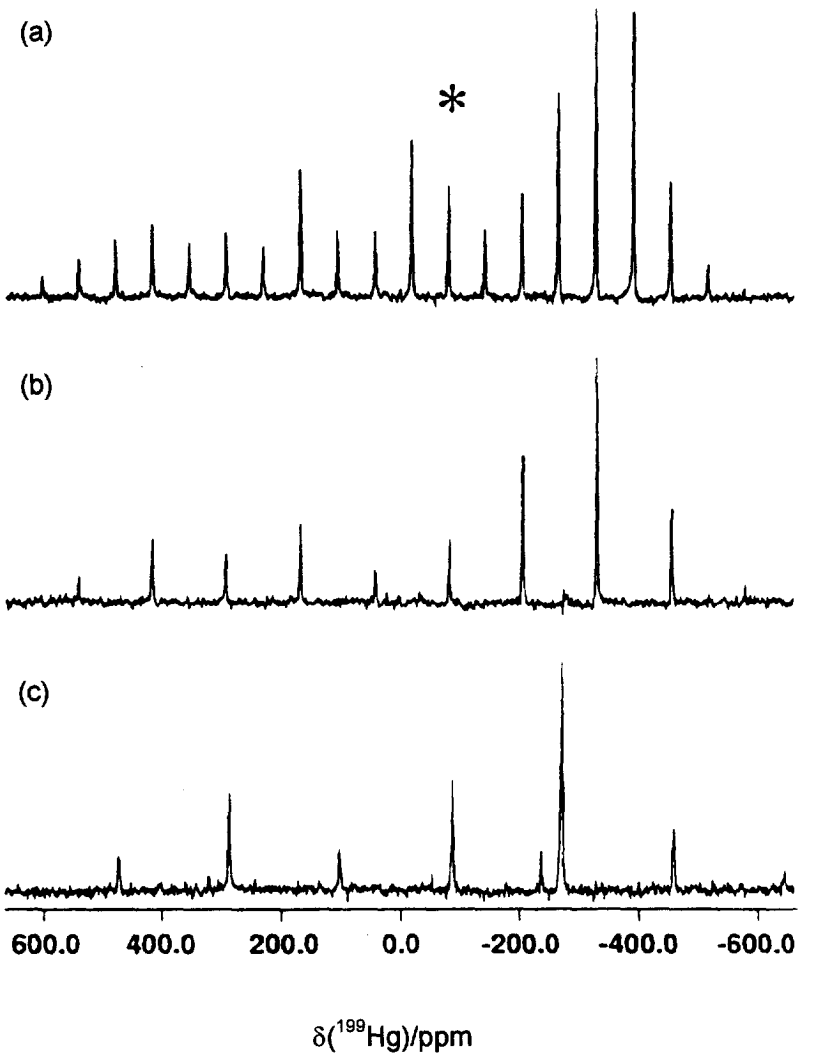

Fig. 2. 64.4 MHz ^{199}Hg CP MAS spectra of $[Me_4N][Hg(S^iPr)_3]$ at spinning speeds of (a) 4, (b) 8 and (c) 12 kHz [reproduced, with permission, from Ref. [64]]. The centreband is marked *.

distribution in the spinning sideband manifold is dependent on these parameters. The centreband is readily identified as the band whose position remains invariant as the spinning frequency is varied. A number of publications have discussed the calculation of the spinning sideband intensities, and also the inverse problem of determining the chemical shift or shielding tensor parameters from experimental sideband patterns [65–73]. The main methods which have been used for the latter problem are moment analysis [65,67,73], the sideband intensity ratio graphical method [66,69,73], or iterative calculations involving simulation of the intensity

distribution over the full sideband manifold [67,70–73]. The last-mentioned method is currently considered to be the most reliable, although the other two may be useful for providing approximate values of the shielding tensor parameters, which can then be refined by means of the iterative procedure [71,73]. One difficulty with sideband analysis methods concerns the cases of axial symmetry ($\eta = 0$) or near-axial symmetry ($\eta \approx 0$). In such situations the anisotropy may be obtained with good accuracy, but the simulated spectrum is very insensitive to the value of η, so that this parameter is not very accurately determined [17,34,67,70]. This is well illustrated by the case of mercury(II) acetate, where the static ^{199}Hg spectrum yields $\eta = 0.08$, but sideband analysis for several different spinning rates yields values in the range 0.00–0.23 [36]. By contrast, however, sideband analysis of the ^{199}Hg spectrum for $[NMe_4][Hg(S^iPr)_3]$, in which the mercury atom lies on a threefold symmetry axis, yielded $\eta = 0.00$ as expected [64,74], showing that values for axial or near-axial η can be determined in favourable cases. A number of publications have considered other factors which determine the accuracy of shielding tensor parameters obtained from spinning sideband analysis [34,69,72,75], including the effects of cross polarization [75], which are discussed in more detail below.

One factor which may affect the accuracy of the parameters obtained by spinning sideband analysis which has not been given much consideration to date is the variation in the degree of polarization of the nuclei over the full frequency range of the spectrum as a result of the finite width of the pulse used in the excitation process, for example in spectra obtained by direct polarization. With lighter nuclei which have small chemical shift anisotropies, the frequency range of the spectrum is small in comparison with the frequency range of the pulse, so this problem does not generally arise. For heavy-metal nuclei such as ^{199}Hg, however, shielding anisotropies $\Delta\sigma = 5000$ ppm or higher can occur, and the question of whether all of the nuclei in the sample are equally excited (or polarized) by the pulse needs to be considered. The frequency distribution of RF magnetic field amplitudes takes the form $\sin[\pi(\nu - \nu_c)\tau_p]/\pi(\nu - \nu_c)\tau_p$ (ν_c = centre frequency; τ_p = pulse duration) for square-wave pulses so that a pulse of duration τ_p has an associated spectral range of the order of $1/\tau_p$ [14]. Since the signal strength is directly proportional to the strength of the radiofrequency field used to bring about the polarization, the distribution of intensities in the spectrum should be modified by the $\sin x/x$ function given above (though phasing complications also exist). The situation for the direct polarization spectrum of $Hg(SCN)_2$ is illustrated in Fig. 3, which shows the spectra obtained by using 1 μs and 6 μs pulses. While the spectra look quite similar, there are differences in the integrated intensities of corresponding sidebands in the spectra. This is indicated more clearly in Fig. 4, which shows the ratios of the intensities of corresponding peaks in the spectra. Also shown in this figure are the theoretical ratios based on the $\sin[\pi(\nu - \nu_c)\tau_p]/\pi(\nu - \nu_c)\tau_p$ factors for the two pulse durations. This shows, for example, that the excitation of the sideband in the most shielded region (sideband number 11) by the 6 μs pulse is only about 30% of that due to the 1 μs pulse. The intensity ratios from the lines in the spectrum show the same general trend as the theoretical prediction, but there are also considerable deviations, presumably due to measurement errors (either in the acquisition or integration processes)

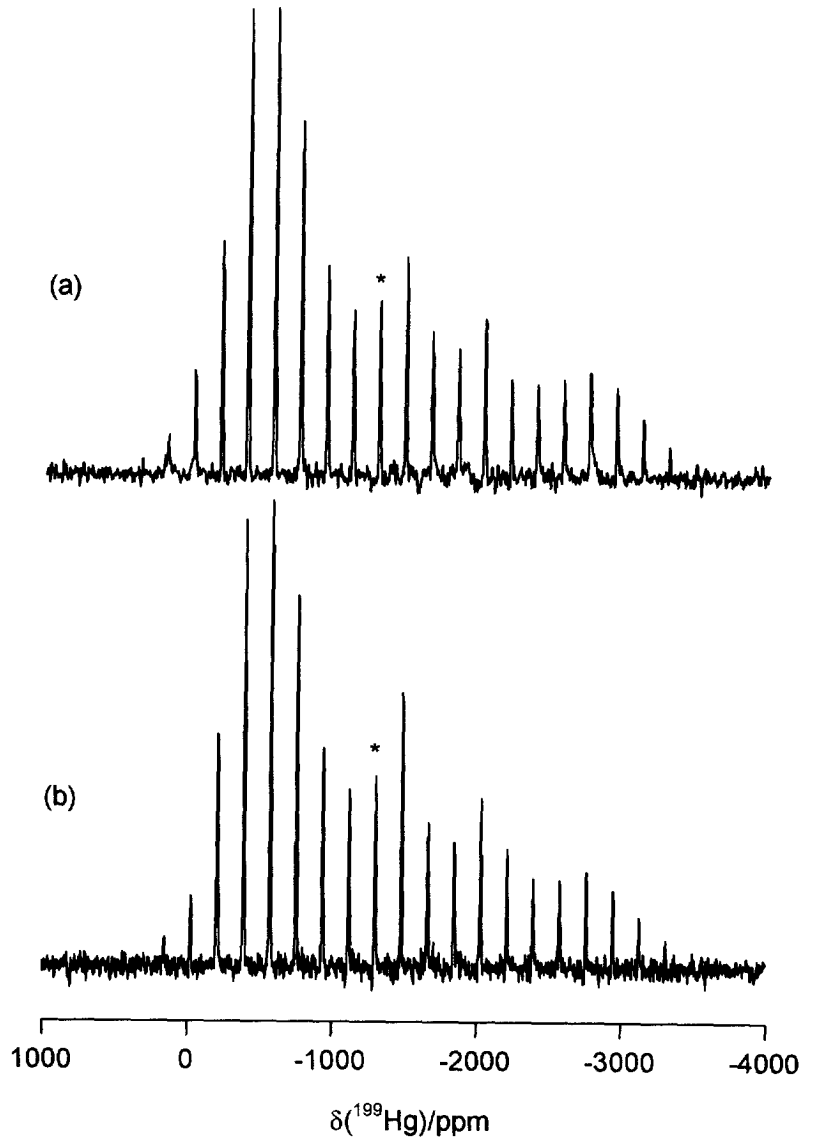

Fig. 3. 53.6 MHz ^{199}Hg MAS spectra of $Hg(SCN)_2$ using pulse angles and durations of (a) 12.9°, 1 μs and (b) 77.1°, 6 μs, respectively.

and/or to the noise levels in the spectra. The intensities can be partially corrected by dividing the individual sideband intensities by the appropriate sin x/x excitation profile, and the effects of this on the calculated shielding tensor parameters are shown in Table 2. As expected, the anisotropy $\Delta\sigma$ and the asymmetry parameter η increase after the correction is applied to the 6 μs spectrum; anything which reduces

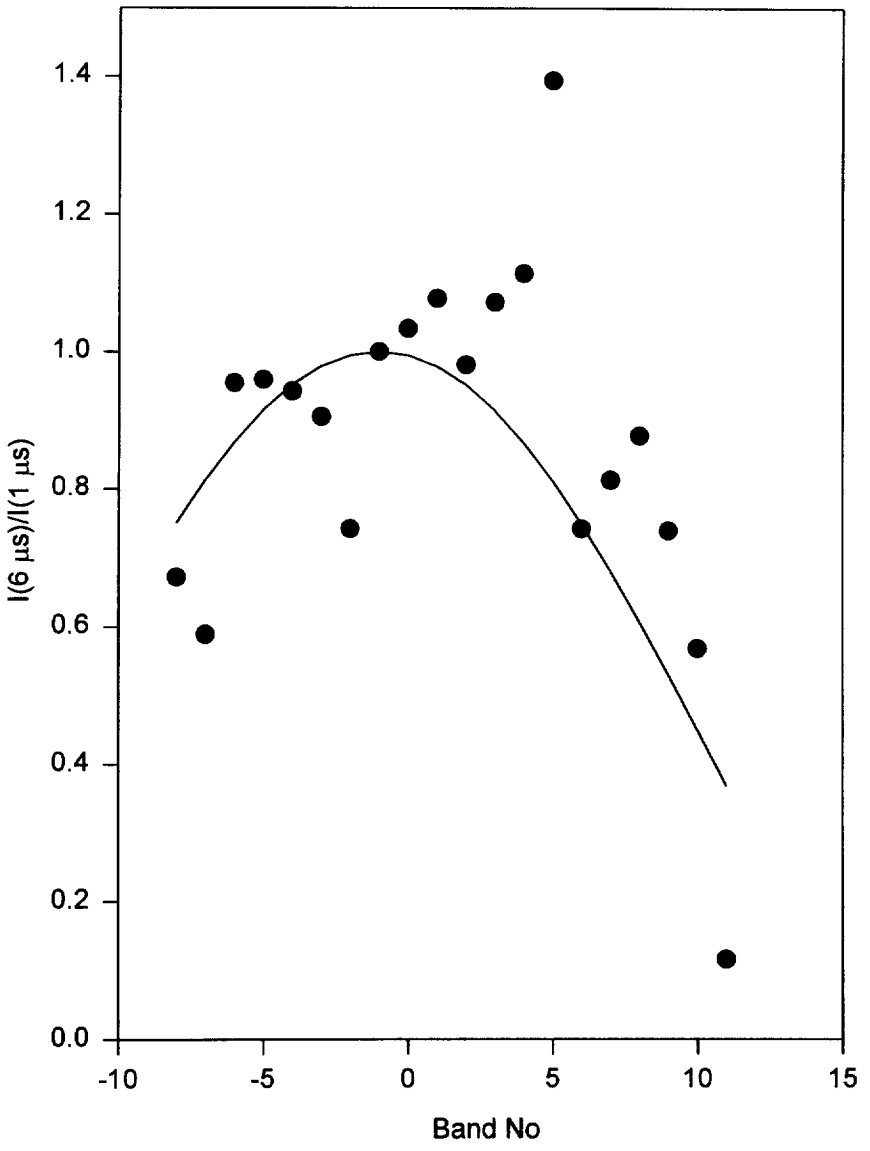

Fig. 4. Ratio of the intensities of corresponding peaks in the 6 μs and 1 μs spectra in Fig. 3. The continuous line shows the theoretical ratio based on the different excitation profiles for the two pulse durations.

the intensity of the outer sidebands in the spectrum relative to the inner ones results in a spectrum which is closer to that for an isotropic system, for which $\Delta\sigma = 0$; $\eta = 0$. The effects of this correction for the 1 μs pulse spectrum are negligible, since the frequency range of this pulse ($1/\tau_p = 1$ MHz) is much greater than the spectral width due to the shielding anisotropy ($\nu_0.\Delta\sigma \approx 0.2$ MHz). For the 6 μs spectrum, the effects

Table 2
Calculated ^{199}Hg shielding tensor parameters for $Hg(SCN)_2$

Conditions	$(\sigma_{11}-\sigma_r)$ (ppm)	$(\sigma_{22}-\sigma_r)$ (ppm)	$(\sigma_{33}-\sigma_r)$ (ppm)	$\Delta\sigma$ (ppm)	η	$(\sum d^2)^a$
6 μs, uncorr.	82(26)	445(23)	3372(30)	3109(45)	0.18(2)	15
6 μs, corr.	42(13)	443(11)	3415(17)	3172(25)	0.19(1)	4
1 μs, uncorr.	81(23)	428(21)	3391(24)	3136(37)	0.17(2)	10
1 μs, corr.	75(19)	436(17)	3388(22)	3133(33)	0.17(1)	8

[a] d = difference between measured and calculated sideband intensities.

of the correction are more significant, although the expectation that the parameters from the corrected spectra for both pulse durations should be the same is not very closely realized due to the experimental errors in the sideband intensities which are evident in the deviations of the intensity ratios from their predicted values (Fig. 4). Nevertheless, the results discussed here show that the pulse duration may have an influence on the shielding parameters obtained from spinning sideband analyses, and that it is important to state the pulse duration used to obtain spectra when reporting the results of such studies, so that the effects of this variable can be assessed.

A further factor which can affect the accuracy of the determination of the shielding tensor components from spinning sideband analysis of MAS in the case of CP MAS spectra is the effect of CP on the intensities of the spinning sidebands. It has been shown that CP MAS spectra show deviations from the intensity distribution of the sideband pattern in comparison with the direct polarization spectra [75]. The evaluation of the principal components of the shielding tensor by sideband analysis thus involves a systematic error. The reason for the sideband intensity deviations is the anisotropic magnetization of the X spins caused by the Hartmann–Hahn mismatch anisotropy, as well as the anisotropic CP rate, and the anisotropic relaxation rate of the ^{1}H spins in the rotating frame. These effects result in a progressive reduction in the intensity of the sidebands with increasing distance of the sideband from the point of irradiation. Two methods were proposed to overcome this problem. The first is a modified pulse sequence called multiple-contact isotropic cross-polarization (MCI CP), while the second involves the use of an empirical intensity correction function. The best correction function was found to be of the form $\sin x/x$ (note that this is the same as the function required for the correction of intensity deviations caused by the finite duration of the excitation pulse in direct polarization experiments, see above). A combination of both of these is recommended to reduce the errors involved in spinning sideband analyses of CP MAS spectra [75]. This approach does not appear to have been applied to the analysis of ^{199}Hg CP MAS spectra, despite the fact that the errors are expected to increase with increasing chemical shift anisotropy [75], and so should be most severe in the case of heavy-metal nucleus NMR.

Relatively few ^{199}Hg MAS spectra have been reported which involve indirect spin–spin coupling to another spin-1/2 nucleus, such as ^{31}P. One such spectrum which has been described recently is the ^{199}Hg CP MAS NMR of

$[Hg(PCy_3)(OAc)_2]$ [58]. This spectrum consists of a centreband and spinning sidebands, all of which are split into doublets by the $^1J(^{199}Hg,^{31}P)$ coupling. The spectrum was analyzed to yield an isotropic spin–spin coupling constant, but no analysis for the anisotropic ^{199}Hg shielding tensor components was given. As discussed in Section 2.3, the $^1J(^{199}Hg,^{31}P)$ coupling would in general be expected to be anisotropic in the solid state, but none of the programs for spinning sideband analysis described above are directly applicable to the general case of combined anisotropic ^{199}Hg shielding and anisotropic spin–spin coupling. Indeed, such an analysis is difficult for a powder sample without some assumption about the relative orientations of the principal axes of the shielding and coupling tensors. However, a discussion of the AX and linear AX_2 systems for the case where the σ and J tensors are axially symmetric and their principal axes lie along the relevant internuclear vector (and perpendicular to it) has been given [76]. For the AX case, for example, it was shown that the two transitions for the A nucleus (one for each of the two possible spin states $m_X = \pm 1/2$ of the X nucleus) have associated sideband manifolds with effective anisotropies

$$\Delta\sigma_A^{eff} = \Delta\sigma_A - (3D'/\nu_A^0)m_X \tag{34}$$

where $D' = D - \Delta J/3$, $\Delta J = J_\parallel - J_\perp$ is the anisotropy in J, and D is the AX dipolar coupling constant, Eq. (26). Analysis for each of the two sideband manifolds (assuming they are distinguishable through J_{iso}) thus yields $\Delta\sigma_A$ and D', including the sign of the latter if that of J_{iso} is known.

In most cases, the results of sideband analysis have been given without any rigorous analysis of the precision of the derived parameters. Frequently, the shielding tensor components are quoted to a precision similar to that corresponding to the location of the NMR line positions, but this approach would only be justified in a static-sample single-crystal study. In MAS studies, the intensities of the bands in the spinning sideband manifold exhibit deviations from the theoretical intensities, due to the presence of noise in the spectrum and other experimental errors, and this will result in errors in the resulting shielding tensor parameters. A procedure for carrying out a rigorous statistical analysis of such errors has recently been published [77]. However, this undoubtedly underestimates the true errors, since there are normally uncorrected systematic errors (see above).

4. Survey of the data

4.1. Anisotropic shielding constants

Prior to the advent of high-resolution solid-state NMR, anisotropic ^{199}Hg shielding constants had been obtained for a few compounds from liquid-crystal spectra or from solution-state relaxation time measurements. These results are summarised in Table 3. These studies provide useful reference data for compounds such as $Hg(CH_3)_2$ which is not a solid under ambient conditions, and whose shielding

Table 3
^{199}Hg chemical shifts and shielding tensor parameters from liquid-crystal spectra or solution-state relaxation time measurements

Compound	$(\sigma_{11}-\sigma_r)$ (ppm)	$(\sigma_{22}-\sigma_r)$ (ppm)	$(\sigma_{33}-\sigma_r)$ (ppm)	δ_{iso} (ppm)	$\Delta\sigma$ (ppm)	η	Ref.
$(Hg(CH_3)_2)^a$	−2442	−2442	4883	0	7325±55	0	[78,79]
$Hg(CH_3)Cl^a$	−1035	−1035	4500	−1155	5535±80	0	[78]
$Hg(CH_3)Br^a$	−908	−908	4550	−910	5455±100	0	[78]
$Hg(CH_3)I^a$	−740	−740	4740	−1085	5480±300	0	[78]
$(Hg(CN)_2)^b$	−30	−30	3770	−1240	3800	0	[80]

[a] From liquid-crystal spectra.
[b] From solution-state relaxation time measurements.

anisotropy is in any case too great to be readily determined by currently available solid-state NMR techniques. They also provide comparative data for compounds (e.g. $Hg(CN)_2$) which have also been studied in the solid state. A summary of the results available to date for compounds which have been studied in the solid state is given in Table 4.

As discussed in Section 2.1, no ab initio calculations of anisotropic ^{199}Hg shielding parameters in mercury compounds appear to have been reported to date. Thus, the interpretation of these parameters remains largely empirical. The discussions which have been published so far are based on essentially qualitative correlations between the shielding parameters and aspects of the mercury coordination environment, such as the mercury coordination number. These correlations will be considered in further detail below. First, however, consideration will be given to possible semi-empirical analyses based on Eqs. (21)–(23). The various structure types to be considered are illustrated in Fig. 5, and for these it can be shown that $p_{ij}=0$ for $i\neq j$, so that Eqs. (21)–(23) can be written in the simpler form

$$\sigma_{xx}=(n_y+n_z-n_yn_z)\sigma_p \tag{35}$$

$$\sigma_{yy}=(n_x+n_z-n_xn_z)\sigma_p \tag{36}$$

$$\sigma_{zz}=(n_x+n_y-n_xn_y)\sigma_p \tag{37}$$

where $n_x=p_{xx}$, $n_y=p_{yy}$, $n_z=p_{zz}$, are the populations of the Hg $6p_x$, $6p_y$, $6p_z$ orbitals, respectively (these populations can take values in the range 0 to 2), and the notations designating these as the local paramagnetic contributions to $\boldsymbol{\sigma}$ have been omitted for clarity.

For linear two-coordinate compounds HgX_2 involving the σ-donor (non π-donor) ligand X, the bonding is influenced by electron donation from the σ-donor orbital of X (or X^- if HgX_2 is a neutral complex) into the Hg $6p_z$ orbital (the z-axis lying along the Hg–X bond direction), and the only non-zero orbital population in Eqs. (35)–(37) is that of the $6p_z$ orbital, n_z. This yields $\sigma_{xx}=\sigma_{yy}=n_z\sigma_p$; $\sigma_{zz}=0$. Since σ_p is negative, Eq. (24), this yields $\sigma_{zz}>\sigma_{xx}=\sigma_{yy}$. If it is assumed that the diamagnetic contributions to the shielding are isotropic, and so contribute equally to all three

principal components of the shielding tensor, the above relationship should also hold for the total shielding constant, i.e. $\sigma_{33} > \sigma_{11} = \sigma_{22}$. Inspection of the results for HgX_2 species such as $Hg(CH_3)_2$, $Hg(CN)_2$, $HgCl_2$ in Tables 3 and 4 shows that the experimental results correspond closely to this relationship; the small deviations from equality of σ_{11} and σ_{22} are due to slight departures from axial symmetry in the solid state.

According to the above analysis, the shielding anisotropy $\Delta\sigma$ (Eq. (6)) for linear HgX_2 is given by $\Delta\sigma = -n_z\sigma_p$. Since σ_p is negative, $\Delta\sigma$ is positive. Thus, $\Delta\sigma$ is proportional to the $6p_z$ population n_z which, in turn, is proportional to the σ-donor strength of the ligand. Therefore, a strong σ-donor ligand, such as CH_3^- will result in a greater n_z than will a weaker σ-donor, such as Cl^-, and so $\Delta\sigma$ is predicted to be greater for $Hg(CH_3)_2$ than for $HgCl_2$. The results in Tables 3 and 4 show that this prediction is confirmed. However, the large observed difference between the $\Delta\sigma$ values for these two compounds may also be partly due to differences in secondary bonding interactions, as will be discussed below.

The above discussion applies essentially unchanged to linear mixed-ligand complexes HgXY. The only difference is that the Hg $6p_z$ orbital population contains contributions from both the X and Y ligands, so that $\Delta\sigma$ for HgXY will be intermediate between the values for HgX_2 and HgY_2. Comparison of the results for $Hg(CH_3)_2$, $HgCl_2$ and $Hg(CH_3)Cl$ in Tables 3 and 4 shows that this relationship is observed experimentally. In fact the $\Delta\sigma$ value for $Hg(CH_3)Cl$ is very close to the arithmetic mean of those for $Hg(CH_3)_2$ and $HgCl_2$, and the above analysis gives a physical basis for this otherwise empirical observation. It is perhaps surprising, therefore, that the $\Delta\sigma$ values reported for $Hg(CH_3)X$ (X = Cl, Br, I) are all equal within experimental error (Table 3); an increase along this series might have been expected due to the increased σ-donor strength of X^- (as a result of the decrease in electronegativity from Cl to I) [81]. This effect is probably related to a similar one involving the ^{201}Hg nuclear quadrupole coupling constants in HgX_2, which show little variation with X (Section 2.4). The quadrupole coupling constant is proportional to the electric field gradient at the Hg nucleus and, for a bonding model of the type discussed above, this is given by $eq = n_z eq_p$ where eq_p is the field gradient due to a single $6p_z$ electron. The fact that the quadrupole coupling in linear MX_2 species is relatively independent of X, despite the increase in the σ-donor strength of X^- with decreasing electronegativity of X, has been shown to be due to an expansion of the $6p_z$ orbital from X = Cl to I [50]. This results in a decrease in eq_p, since this quantity is proportional to $\langle r^{-3}\rangle_{6p}$, which compensates for the increase in n_z so that eq remains essentially independent of X. Basically the same situation is expected for the shielding anisotropy $\Delta\sigma = -n_z\sigma_p$, since σ_p is also proportional to $\langle r^{-3}\rangle_{6p}$, Eq. (24), thus providing a possible explanation for the apparent independence of $\Delta\sigma$ on X in $Hg(CH_3)X$.

The type of analysis described above for linear HgX_2 species can also be applied to planar three-coordinate HgX_3 compounds. For the case in which all three Hg–X bonds are symmetrically equivalent, the Hg 6p orbital populations are $n_x = n_y$; $n_z = 0$ (the x, y axes lie in the HgX_3 plane; z is perpendicular to this plane). Substitution into Eqs. (35)–(37) yields $\sigma_{xx} = \sigma_{yy} = n_x\sigma_p$; $\sigma_{zz} = (2n_x - n_x^2)\sigma_p$. The

Table 4
^{199}Hg chemical shift and shielding tensor parameters from solid-state ^{199}Hg NMR spectra

Compound[a]	$(\sigma_{11}-\sigma_r)$ (ppm)	$(\sigma_{22}-\sigma_r)$ (ppm)	$(\sigma_{33}-\sigma_r)$ (ppm)	δ_{iso} (ppm)	$\Delta\sigma$ (ppm)	η	Ω (ppm)	κ	Ref.
$(Hg(CN)_2)$[b]	193±5	223±5	3310±480	−1240±150[c]	3100±480[d]	~0	3117	0.98	[81]
$Hg(CN)_2$	33	381	3773	−1396	3566	0.15	3740	0.81	[82]
$(HgCl_2)$[b]	410±15	410±15	3800±170	−1540±170[c]	3390±170[d]	0	3390	1	[81]
$HgCl_2$	282	573	4019	−1625	3592	0.12	3737	0.84	[82]
$Hg(SCN)_2$	81	428	3390	−1300	3135	0.17	3309	0.79	[83]
$Hg(SeCN)_2$	503	1337	3440	−1760	2520	0.50	2937	0.43	[83]
$(Hg(OAc)_2)$[b]	1870	1968	3651	−2497	1731	0.08	1781	0.89	[36]
$Hg(OAc)_2$	1770	2106	3594	−2490	1656	0.30	1824	0.63	[84]
	1897	1907	3666	−2490	1764	0.0	1769	0.99	[58]
	1859	1947	3685	−2497	1782	0.07	1826	0.90	[85]
$Hg(La)_2$	1996	2277	2984	−2419	847	0.50	988	0.43	[36]
$(Hg_3(Ci)_2)$[e]	1773	1881	3385	−2346	1558	0.10	1612	0.87	[36]
	1772	1839	3465	−2358	1660	0.06	1693	0.92	
	1731	1945	3531	−2402	1694	0.19	1800	0.76	
$Hg(Ph)_2$	−1122	−699	4307	−829	5218	0.12	5429	0.84	[58]
$Hg(^iPr)Cl$[b]	−320±20	−220±20	3930±90	−1130±10[c]	4200±90[d]	~0	4250	0.95	[81]
$Hg(CH_3)I$	−863	−434	3699	−801	4347	0.15	4562	0.81	[86]
Hg(Ph)OAc	187	375	3935	−1499	3654	0.08	3748	0.90	[58]
	47	534	3919	−1500	3629	0.20	3872	0.75	[82]
$Hg(CH_3)OAc$	−433	−34	3948	−1160	4182	0.14	4381	0.82	[82]
Hg(Cl)OAc[e]	827	888	3837	−1850	2981	0.03	3010	0.96	[82]
	880	1051	3795	−1909	2831	0.09	2915	0.88	
Hg(SCN)OAc	770	1035	3481	−1762	2579	0.15	2711	0.80	[82]
Hg(CN)OAc	800	830	3724	−1785	2909	0.02	2924	0.98	[82]
$Hg(OAc)_2(PCy_3)$	–	–	–	−1149	–	–	–	–	[58]
$[Hg(S\text{-}2,4,6\text{-}^iPr_3C_6H_2)_2]$	−627	−180	3852	−1015	4256	0.16	4479	0.80	[60]
$[PPh_4][Hg(S\text{-}2,4,6\text{-}^iPr_3C_6H_2)_3]$	876[f]	596	−672[f]	−267	−1408	0.30	1548	−0.64	[60]
$[PPh_4][Hg(S\text{-}2,3,5,6\text{-}Me_4C_6H)_3]$[g]	1153[f]	275	−685[f]	−247	−1399	0.94	1838	−0.04	[60]
	1057[f]	371	−601[f]	−276	−1315	0.78	1658	−0.17	
$[N^nBu_4][Hg(SPh)_3]$	−494	326	1190	−341	1273	0.97	1684	0.03	[60]
$[NEt_4][Hg(S^tBu)_3]$	−316	83	704	−158	821	0.73	1020	0.22	[84]

Table 4 (*continued*)

Compound[a]	$(\sigma_{11}-\sigma_r)$ (ppm)	$(\sigma_{22}-\sigma_r)$ (ppm)	$(\sigma_{33}-\sigma_r)$ (ppm)	δ_{iso} (ppm)	$\Delta\sigma$ (ppm)	η	Ω (ppm)	κ	Ref.
$[NMe_4][Hg(S^iPr)_3]$	433[f]	433	−629[f]	−79	−1062	0.00	1062	−1.00	[64,74]
$[NEt_4]_2[Hg(S\text{-}2\text{-}PhC_6H_4)_4]$	379	429	491	−433	87	0.86	112	0.11	[60]
$[NMe_4]_2[Hg(SC_6H_4Cl)_4]$	424	428	602	−485	176	0.03	178	0.96	[84]
$Hg(S^tBu)_2$	454	557	984	−665	478	0.32	530	0.61	[84]
$[NMe_4]_2[Hg_2(SPh)_6]$[e]	−105	444	1315	−551	1145	0.72	1420	0.23	[74]
	−92	453	1359	−574	1178	0.69	1451	0.25	
$K_2[Hg(CN)_4]$	463	463	463	−463	0	–	0	–	[87]
$Na[NEt_4][Hg(CN)_4]$	434	434	434	−434	0	–	0	–	[85]
$[NH_4]_2[Hg(SCN)_4]$	355	655	1111	−707	606	0.74	756	0.21	[85]
$[NMe_4]_2[Hg(SCN)_4]$	–	–	–	−585	–	–	–	–	[85]
$[N^nBu_4]_2[Hg(SCN)_4]$	695[f]	695	454[f]	−615	−241	0.0	241	−1.00	[85]
$K_2[Hg(SCN)_4]$	505	581	765	−617	222	0.51	260	0.42	[83]
$Cs_2[Hg(SCN)_4]$	384	572	996	−651	518	0.54	612	0.39	[83]
$K[Hg(SCN)_3]$	−49	323	1941	−738	1805	0.31	1990	0.63	[83]
$Cs[Hg(SCN)_3]$[e]	1623[f]	891	−183[f]	−777	−1440	0.76	1806	−0.19	[83]
	1706[f]	879	−43[f]	−847	−1335	0.93	1749	−0.05	
[Hg(MeS)L]	−208	95	2457	−781	2514	0.18	2665	0.77	[88]
[Hg(EtS)L]	−170	125	2514	−823	2537	0.17	2684	0.78	[88]
$[Hg(dmso)_6][CF_3SO_3]_2$	2354[f]	2354	2232[f]	−2313	−122	0.00	122	−1.00	[37]
$Hg_2(NO_3)_2.2H_2O$[h]	435.2	496.7	3669.3	−1533.7	3203	0.03	3234.1	0.96	[55]
$Hg(SO_4).H_2O$	2876[f]	2665	2086[f]	−2542	−684	0.46	790	−0.47	[86]
$Hg_3(PO_4)_2.2H_2O$[e]	1838	2135	3229	−2401	1244	0.36	1391	0.57	[86]
	1683	2067	3293	−2348	1419	0.41	1610	0.52	
	1629	2080	3022	−2244	1167	0.58	1393	0.35	

[a] Abbreviations: La = lactate; Ci = citrate; L = tris(3,5-dimethylpyrazol-1-yl)hydroborate; dmso = dimethylsulphoxide.
[b] Static (non-rotating) sample.
[c] Average values from solution-state spectra.
[d] Calculated by using isotropic shielding parameters from solution spectra.
[e] Multiple signals due to site inequivalence.
[f] The components σ_{11} and σ_{33} are interchanged for the calculation of Ω and κ, according to Eq. (12).
[g] Two different crystalline phases.
[h] Static single-crystal measurement.

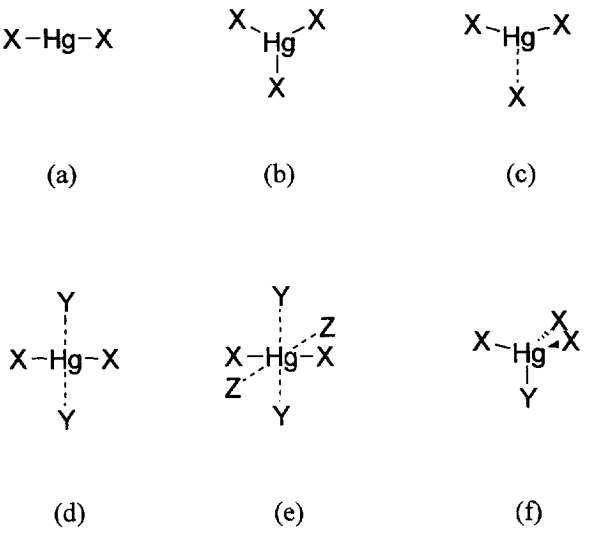

Fig. 5. Coordination environments in some mercury(II) complexes: (a) linear, (b) trigonal planar, (c) distorted trigonal planar, (d) linear with two perpendicular secondary bonding interactions, (e) linear with four mutually perpendicular secondary bonding interactions, (f) pseudo-tetrahedral.

shielding anisotropy is thus $\Delta\sigma = n_x(1-n_x)\sigma_p$. Unlike the linear two-coordinate case, for which $\Delta\sigma$ is always positive, $\Delta\sigma$ for the trigonal planar case may be positive or negative depending on whether n_x $(=n_y)$ is greater or less than 1. The only complex having a perfectly trigonal planar mercury environment for which shielding anisotropy data are available is $[Hg(S^iPr)_3]^-$ (Table 4) [64,74]. For this complex, $\Delta\sigma$ is negative, implying that n_x $(=n_y) < 1$. This is chemically reasonable; for pure covalent metal–ligand bonding involving sp^2 hybrid orbitals on mercury, $n_x = n_y = 1$, but these populations are expected to be less than this limiting value in practice because (a) the degree of ligand-to-metal charge transfer will generally be less than that required for a pure covalent bond, and (b) the Hg 6s orbital is lower in energy than the Hg 6p orbitals, so that more electron density will reside in the s orbital than in the p orbitals, compared with the values predicted on the basis of ideal sp^2 hybridization. This is demonstrated in the closely related system $[AuCl_2]^-$ (isoelectronic with $HgCl_2$), for which the 6s and $6p_z$ orbital populations have been calculated to be 0.86 and 0.33 respectively [50], compared with equal populations predicted by the sp hybridization model. There is thus a distinct and diagnostic difference between the Hg shielding anisotropies for linear and trigonal coordination; $\Delta\sigma$ should normally be positive for the linear HgX_2 geometry and negative for the trigonal planar HgX_3 geometry, in good agreement with the experimental observations. Thus, for example, $\Delta\sigma$ for $[Hg(S\text{-}2,4,6\text{-}^iPr_3C_6H_2)_2]$ (linear HgS_2 coordination) is positive, whereas that for $[Hg(S^iPr)_3]^-$ (trigonal planar HgS_3 coordination) is negative (Table 4) [64,74].

Exact trigonal planar HgX_3 coordination is rare, and $[Hg(S^iPr)_3]^-$ is the only case for which ^{199}Hg shielding anisotropy data are available. There are, however,

several examples of distorted trigonal planar coordination in which one of the X ligands is more weakly bonded than the other two. In order to investigate the consequences of such a distortion on the shielding parameters, calculations based on a simple model have been carried out. In this model the HgX_3 unit lies in the xy plane, with one of the HgX bonds lying along the y-axis. The populations of the Hg $6p_x$ and $6p_y$ orbitals in the symmetrical HgX_3 case are equal, and are set to n. The distortion involving a weakening of the Hg–X bond along the y direction is represented by a reduction in the population of the $6p_y$ orbital by a factor r, so that it is rn. Substitution of the populations into Eqs. (35)–(37) yields $\sigma_{xx}=rn\sigma_p$; $\sigma_{yy}=n\sigma_p$; $\sigma_{zz}=(n+rn-rn^2)\sigma_p$. According to the definition (Eq. (5)), $\sigma_{11}=\sigma_{xx}$; $\sigma_{22}=\sigma_{yy}$; $\sigma_{33}=\sigma_{zz}$ for $r>1/(2-n)$. The resulting expressions for the shielding anisotropy and asymmetry parameters are

$$\Delta\sigma=(n/2)[r(1-2n)+1]\sigma_p \tag{38}$$

$$\eta=3(1-r)/(1+r-2rn) \tag{39}$$

For $r<1/(2-n)$, the definition (Eq. (5)) yields $\sigma_{11}=\sigma_{zz}$; $\sigma_{22}=\sigma_{yy}$; $\sigma_{33}=\sigma_{xx}$, so that

$$\Delta\sigma=(n/2)[r(1+n)-2]\sigma_p \tag{40}$$

$$\eta=3r(1-n)/(2-r-rn) \tag{41}$$

The dependence of $\Delta\sigma$ and η on r according to Eqs. (38)–(41) for the case $n=0.5$ is shown in Fig. 6. A geometry change is associated with the change in r. The region near $r=1$ corresponds to a small distortion of trigonal HgX_3 towards a C_{2v} X_2Hg–X structure; a decrease in r corresponds to an increase in the degree of distortion. Associated with this distortion is an increase in the X–Hg–X angle of the X_2Hg unit so that this angle becomes 180° when $r=0$. The change in the form of the ^{199}Hg spectrum with change in r is illustrated in Fig. 7.

An important aspect of Eq. (38) is its relative independence on r. In fact, for a population $n=0.5$, $\Delta\sigma$ is completely independent of r. The results in Fig. 6 show that in this region $\Delta\sigma$ is quite insensitive to the degree of distortion from the trigonal structure, whereas η is strongly affected by it. This appears to correspond well with experimental observations for distorted three-coordinate compounds. Thus, for example, the complex $[Hg(S\text{-}2,3,5,6\text{-}Me_4C_6H)_3]^-$, which contains an HgS_3 coordination environment distorted in the sense described above [60], yields $\Delta\sigma\approx -1400$ ppm and $\eta\approx 0.9$ (Table 4). By contrast, the closely-related complex $[Hg(S\text{-}2,4,6\text{-}{}^iPr_3C_6H_2)_3]^-$, which has almost perfect trigonal planar HgS_3 coordination [60], also yields $\Delta\sigma\approx -1400$ ppm, but gives a considerably lower asymmetry parameter $\eta\approx 0.3$ (Table 4). Thus, the prediction from Fig. 6 that η is a much more sensitive indicator of distortion from trigonal planar coordination than $\Delta\sigma$ appears to be borne out by experiment. Fig. 6 also predicts that beyond a certain point in the distortion ($r=2/3$ in this example) the sign of $\Delta\sigma$ switches from negative to positive, while η remains close to 1. This appears to occur in the case of the complex $[Hg(SPh)_3]^-$, which shows a slightly greater degree of distortion than that in $[Hg(S\text{-}2,3,5,6\text{-}Me_4C_6H)_3]^-$ [60], and which yields $\Delta\sigma\approx 1273$ ppm, $\eta\approx 0.97$ (Table 4).

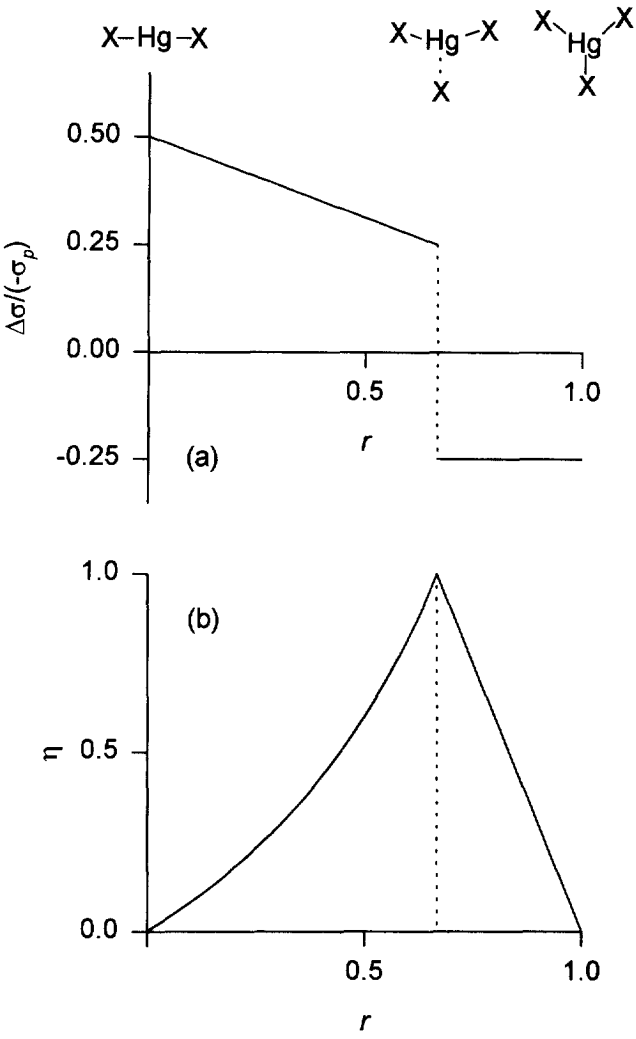

Fig. 6. The dependence of (a) $\Delta\sigma$ and (b) η on r according to Eqs. (38)–(41) for the case $n=0.5$ (for details see text).

The switch in the sign of $\Delta\sigma$ might suggest at first sight a rather dramatic difference between the structures or electronic configurations in these two compounds, but this is not the case. The principal components of the shielding tensor change continuously with r, but at the point where the relative magnitudes of $\sigma_{xx}-\sigma_{iso}$ and $\sigma_{zz}-\sigma_{iso}$ are reversed, σ_{11} and σ_{33} are interchanged according to Eq. (5) and an apparent discontinuity in $\Delta\sigma$ occurs, which is an artefact of the definitions of the shielding components.

An alternative way of describing the anisotropic ^{199}Hg shielding parameters is via the span and skew (Eqs. (15) and (17)), as described earlier in this review. The

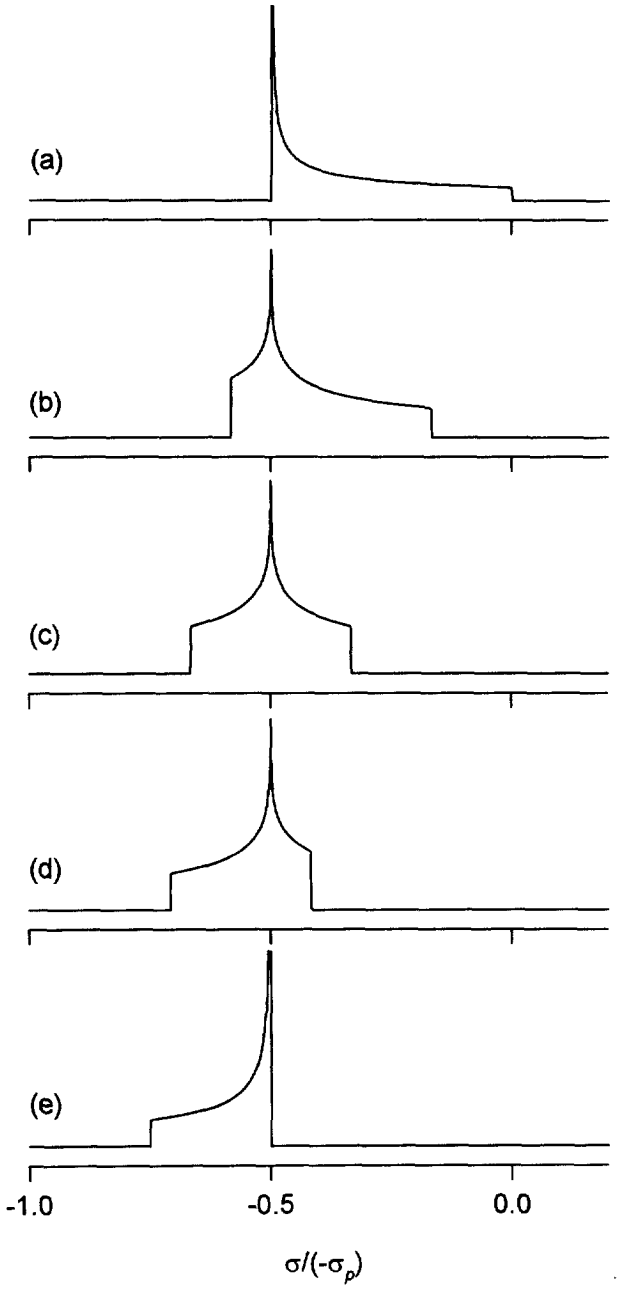

Fig. 7. Solid-state ^{199}Hg NMR spectra corresponding to the cases in Fig. 6 at (a) $r=0$ (linear HgX_2 coordination; $\Delta\sigma$ +ve, $\eta=0$), (b) $r=0.33$ (X–HgX_2 coordination; $\Delta\sigma$ +ve, $\eta=0.33$), (c) $r=0.67$ (X–HgX_2 coordination; $\eta=1$), (d) $r=0.83$ (X–HgX_2 coordination; $\Delta\sigma$ −ve, $\eta=0.5$) and (e) $r=1$ (trigonal HgX_3 coordination; $\Delta\sigma$ −ve, $\eta=0$).

cases of linear and ideal trigonal coordination both involve axial symmetry ($\eta=0$), and these yield $\Omega=|\Delta\sigma|$ and $\kappa=+1$ (linear) or $\kappa=-1$ (trigonal). For the model of the C_{2v} distorted X_2Hg–X structure discussed above, the definition (Eq. (16)) corresponds to $\sigma_{11}=\sigma_{zz}$; $\sigma_{22}=\sigma_{yy}$; $\sigma_{33}=\sigma_{xx}$ for all r ($0\leq r\leq 1$), and the equations corresponding to Eqs. (38)–(41) are as follows

$$\Omega=n(rn-1)\sigma_p \tag{42}$$

$$\kappa=(1-2r+rn)/(1-rn) \tag{43}$$

The variation of the shielding tensor components σ_{11}, σ_{22}, σ_{33} and the parameters Ω and κ for the case $n=0.5$ are shown in Fig. 8. This shows that Ω changes continuously from $-0.5\sigma_p$ for linear coordination to $-0.25\sigma_p$ for trigonal coordination, while κ changes continuously from $+1$ for linear coordination to -1 for trigonal coordination. Naturally, the change in the sign of κ occurs under exactly the same conditions as the change in sign of $\Delta\sigma$; compare Figs. 6b and 8c. This is also evident from the values of these parameters for several of the compounds listed in Table 4.

Linear two-coordinate complexes HgX_2 often show secondary bonding interactions to ligands which lie perpendicular to the X–Hg–X axis (the z-axis). For the case of an interaction with a single ligand Y which lies on a twofold axis passing through the Hg atom (the y-axis), the $6p_z$ orbital has a population n due to bonding with the two X ligands, and the $6p_y$ orbital has a small population due to bonding with the Y ligand. If the $6p_y$ population is set equal to rn, then this situation corresponds to the one already discussed above for the strongly distorted trigonal coordination case, which results in Eqs. (40) and (41). The isolated linear HgX_2 case corresponds to $r=0$, and this results in a large positive $\Delta\sigma$ and $\eta=0$ as expected (Fig. 6). For weak interactions with the third ligand Y, $r\ll 1$, and this results in a decrease in $\Delta\sigma$ and an increase in η (Fig. 6). Note the contrast with the case of distortion of HgX_3 from D_{3h} symmetry ($r\approx 1$), where $\Delta\sigma$ is quite insensitive to the degree of distortion. The analysis for the case of a linear HgX_2 unit involved in secondary bonding to two ligands Y which lie on the y-axis and on opposite sides of the Hg atom is essentially the same as the case already discussed above for the interaction with a single ligand Y, and solid $Hg(SeCN)_2$ may be considered as an example of this situation. The primary bonding involves two strong, collinear Hg–Se bonds, but there are two secondary Hg–Se interactions perpendicular to the main Se–Hg–Se unit [83]. This results in $\Delta\sigma=2520$ ppm, $\eta=0.50$ (Table 4). This can be compared with the case of $Hg(SCN)_2$, in which there are no secondary Hg–S interactions [83], and which yields $\Delta\sigma=3136$ ppm, $\eta=0.17$ (Table 4). The decrease in $\Delta\sigma$ and the increase in η resulting from the secondary Hg–Se interactions in $Hg(SeCN)_2$ are entirely consistent with the predictions in Fig. 6. The situation for the above two compounds is complicated slightly by the presence of Hg–N interactions in both cases, but these are considered to be weaker than the Hg–Se interactions [83], and are neglected in this discussion.

In several cases of linear HgX_2 coordination involving secondary bonding, the asymmetry parameter remains close to zero due to the fact that four ligands are

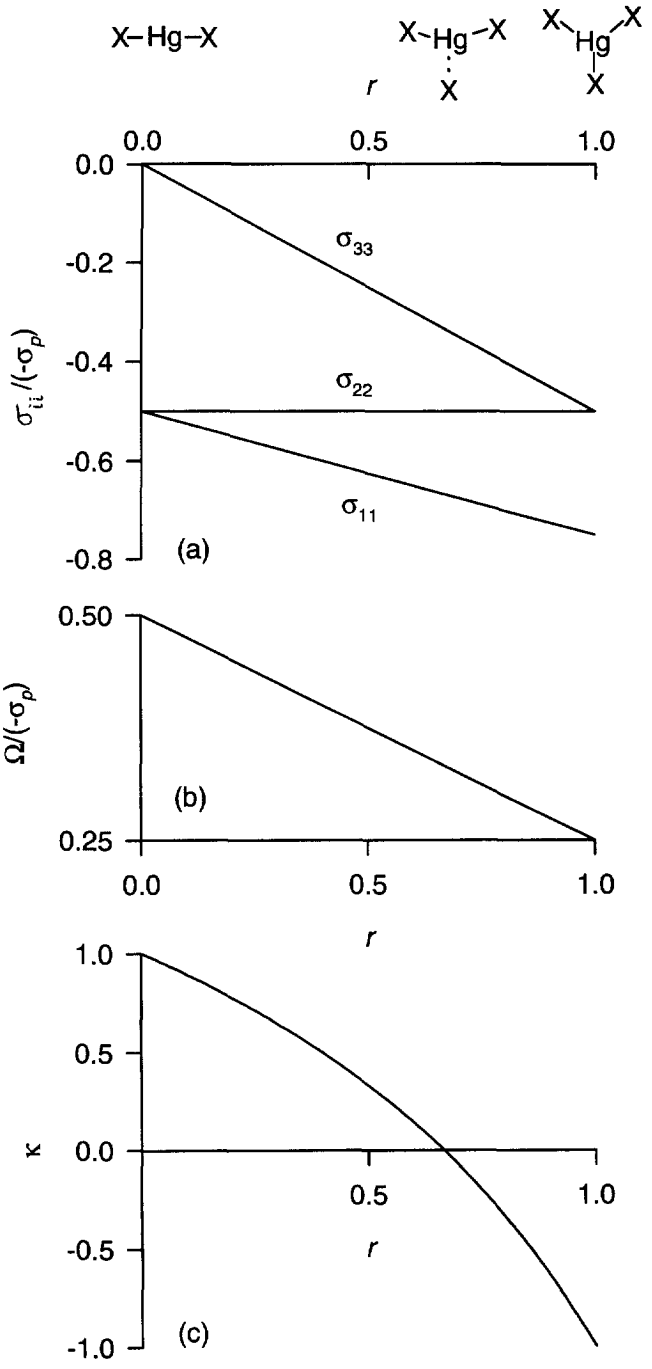

Fig. 8. The dependence of (a) σ_{11}, σ_{22}, σ_{33}, (b) Ω and (c) κ on r according to Eqs. (42) and (43) for the case $n=0.5$ (for details see text).

involved in the secondary bonding, symmetrically disposed about the X–Hg–X axis. This situation can be modelled by a linear HgX_2 unit along the z-axis with secondary bonding to four ligands Y symmetrically placed along the x- and y- axes. The only modification required to the above treatment is that both the $6p_x$ and $6p_y$ orbitals have populations rn. This yields

$$\Delta\sigma = -n(1-r)(1-rn)\sigma_p \tag{44}$$

An important feature of this equation is its quadratic dependence on r. In fact $\Delta\sigma$ is approximately proportional to $(1-r)^2$ and this means that, for small r, $\Delta\sigma$ decreases rapidly with r, the rate of decrease being approximately twice that which would occur if the dependence on r were linear. This means that $\Delta\sigma$ is unusually sensitive to the presence of secondary interactions of this type, an observation which has been made before but has hitherto not been explained [10]. The origin of the quadratic dependence of $\Delta\sigma$ on r is the presence of the binary terms involving products of orbital populations ($n_x n_y$ etc.) in Eqs. (35)–(37). Other physical properties do not display such a high sensitivity to the secondary bonding interactions. For example, the ^{201}Hg quadrupole coupling constant, like the local paramagnetic shielding, depends on the Hg 6p orbital populations, and equations similar to Eqs. (35)–(37) can be written for the electric field gradient tensor components. However, these equations contain no cross terms involving the orbital populations, and the quadrupole coupling constant is predicted to show only a linear dependence on $(1-r)$.

One method of assessing the effects of secondary bonding in the solid state on the ^{199}Hg shielding parameters is to compare the parameters for a particular compound in the solid and solution states. So far, the only compounds for which such data are available are $Hg(CN)_2$ [80,82] and $Hg(CH_3)I$ [78,86]. In both cases a decrease in $\Delta\sigma$ is observed from the solution to the solid state (Tables 3 and 4), implying that secondary bonding interactions in the solid are stronger than those in solution. Confirmation of this conclusion in the case of $Hg(CH_3)I$ can be obtained from Raman measurements, which show that the ν(HgX) and ν(HgC) vibrational modes occur at lower frequency in the solid than in solutions of this compound in a range of different solvents [89].

The case of ideal tetrahedral HgX_4 coordination is a particularly simple one; the populations n_x, n_y, n_z are all equal in this case, and Eqs. (35)–(37) show that all three principal components of the shielding tensor should be the same, so that $\Delta\sigma = 0$; $\eta = 0$. The only cases reported to date which show no detectable departure from isotropic ^{199}Hg shielding are for $[Hg(CN)_4]^{2-}$ complexes in which the Hg atoms occupy crystallographic sites of cubic symmetry [85,87]. However, $\Delta\sigma$ values for several complexes of the type $[HgL_4]^{2-}$ (L = S-donor ligand) lie in the range -241 to 606 ppm (Table 4). These non-zero $\Delta\sigma$ values must arise from distortions of the HgS_4 environment from ideal tetrahedral geometry. In fact, ideal T_d symmetry is not compatible with the non-linear Hg–S–C geometry which occurs in these complexes, but the low value of $\Delta\sigma$ found for $K_2[Hg(SCN)_4]$ shows that this is not the primary cause of the relatively large $\Delta\sigma$ values in the other complexes with HgS_4

coordination environments [83]. It appears that $\Delta\sigma$ and η are determined primarily by the arrangement of the atoms directly bonded to the Hg atom, and that the position of the other atoms in the ligands plays a relatively minor role. In $Hg(S^tBu)_2$, the Hg atoms are present in a distorted HgS_4 coordination environment, the Hg atoms being linked in one-dimensional chains by pairs of doubly-bridging thiolate ligands. The $\Delta\sigma$ value for this case lies within the range quoted above for HgS_4 coordination. The η values vary over the wide range 0–0.9 in the above examples involving distorted HgS_4 coordination, and there is no simple relationship between the $\Delta\sigma$ and η values. This is not unexpected, since a variety of different kinds of distortion from the ideal tetrahedral HgS_4 environment are possible, and no attempt has yet been made to correlate these with the shielding anisotropy and asymmetry parameters.

A somewhat larger distortion from tetrahedral coordination geometry occurs in $[Hg_2(SPh)_6]^{2-}$, in which each mercury atom is bound to two terminal and two bridging thiolate ligands, and this is reflected in the larger $\Delta\sigma$ value of about 1160 ppm [74]. The distortion is such that the S–Hg–S angle involving the terminal thiolate ligands (132°) is considerably greater than the tetrahedral angle (110°). The structure can be considered to be intermediate between one involving ideal tetrahedral coordination at the Hg atoms and one involving two linearly coordinated Hg atoms in which only the terminal thiolate ligands remain bound, the two bridging ligands having been removed from the coordination environment. It has been noted that the anisotropy parameter $\Delta\sigma$ provides a measure of the extent of the distortion from ideal tetrahedral coordination [74]. The $\Delta\sigma$ value is 27% of that for the linear two-coordinate complex $[Hg(S\text{-}2,4,6\text{-}^iPr_3C_6H_2)_2]$, whereas the S–Hg–S bond angle (132°) is greater than the tetrahedral angle by 22° which is about 30% of the total increase of 70° (110 to 180°) involved in the transition from tetrahedral to linear coordination.

The complexes [Hg(MeS)L] and [Hg(EtS)L] (L = tris(3,5-dimethylpyrazol-1-yl)hydroborate) are examples of four-coordinate complexes involving mixed ligands. The ligand L provides three N-donor sites, and the fourth coordination site is occupied by the thiolate (S-donor) ligand. An N_3HgS coordination environment of local C_3 symmetry was proposed on the basis of the solid-state ^{199}Hg NMR results [88]. Some idea of the factors which determine the magnitude and sign of the shielding anisotropy can be obtained by means of an analysis based on Eqs. (35)–(37) and a simplified model of the bonding in the X_3HgY unit. This model involves four sp^3 hybrid orbitals, three of which have an occupation a due to the Hg–X bonding, and one of which has an occupation b due to the Hg–Y bond. The Hg 6p orbital populations are $n_x = n_y = a$; $n_z = (a + 3b)/4$, yielding

$$\Delta\sigma = 3/4(a-b)(1-a)\sigma_p \tag{45}$$

Since σ_p is negative, $\Delta\sigma$ is positive if $b > a$. This will be the case if Y is a stronger σ-donor than X, as is expected to be the case for the mixed pyrazolylborate/thiolate (N_3HgS coordination) complexes discussed above, since mercury has a particularly strong affinity for thiolate ligands [26,27]. This is consistent with the large positive

$\Delta\sigma$ values observed for these complexes. The above treatment assumes that all of the angles in the model X_3HgY system are equal to the tetrahedral angle. If this restriction is lifted while still maintaining the overall C_3 symmetry, by setting all three X–Hg–X angles equal to α, then the only change is that the factor 3/4 in Eq. (45) is replaced by $-3\cos\alpha/(1-\cos\alpha)$. This factor will remain positive unless the distortion from tetrahedral geometry is sufficiently great to reduce α to a value less than 90°.

Clearly the analyses described above, based on Eqs. (35)–(37), contain several approximations and assumptions. The most severe limitation involved in these equations is the average excitation energy approximation, and the success of the present approach suggests that ΔE does not vary much between the complexes concerned. Further work is required to establish whether this is the case. However, the fact that so many of the experimental observations can be rationalized by means of this approach lends support to the hypothesis that the shielding anisotropy and asymmetry parameters are dominated by variations in the orbital population factors of the local paramagnetic terms, and suggests that at least a semi-quantitative approach to the interpretation of these parameters is possible, resulting in useful insights. Several more empirical discussions of the correlation between the anisotropic ^{199}Hg shielding parameters and the structures of mercury complexes, mostly dealing with complexes involving S-donor ligands, have been reported in the past [10,60,84]. A number of the points covered in the above treatment are inherent in these correlations, e.g. the decrease in the magnitude of $\Delta\sigma$ from linear MX_2 through trigonal planar MX_3 to tetrahedral MX_4 coordination. However, there are inconsistencies in the sign conventions for $\Delta\sigma$ between different studies which tend to obscure important points such as the change in sign which occurs in this quantity (as defined herein) in going from linear to trigonal planar geometry. On the other hand, the main conclusion from these correlations, namely that the anisotropic ^{199}Hg shielding parameters are capable of yielding information about structure and bonding in mercury complexes, is certainly valid and is further supported by the more detailed analyses presented in the present review.

4.2. *Isotropic shielding constants*

According to Eqs. (35)–(37), the isotropic shielding due to the local paramagnetic term is

$$\sigma_{iso} = (1/3)[2n_x + 2n_y + 2n_z - n_x n_y - n_y n_z - n_x n_z]\sigma_p \tag{46}$$

The main idealised structure types and associated 6p orbital populations normally encountered in mercury complexes are: linear HgX_2 ($n_x = n_y = 0$; $n_z = n$); trigonal planar HgX_3 ($n_x = n_y = n$; $n_z = 0$); and tetrahedral HgX_4 ($n_x = n_y = n_z = n$). Substitution into Eq. (46) yields the following relationships for $0 < n < 1$: $\sigma_{iso}(HgX_2) \gg \sigma_{iso}(HgX_3) > \sigma_{iso}(HgX_4)$, with the latter two becoming equal for populations $n = 1$. The prediction that linear HgX_2 complexes will show the greatest isotropic shielding is well borne out by the results in Table 4, but the isotropic shieldings for

HgX_4 species are generally greater than those for HgX_3. This is probably due to the fact that, as the mercury coordination number increases, the Hg–X bonds become weaker, so that the populations n decrease with increasing coordination number for a given ligand type X. Since the predicted isotropic shieldings for HgX_3 and HgX_4 are not very different for $n>0.5$, it is possible that the decrease in n from HgX_3 and HgX_4 is sufficient to reverse the order of σ_{iso} for these cases, resulting in the experimentally observed order $\sigma_{iso}(HgX_2) \gg \sigma_{iso}(HgX_3) < \sigma_{iso}(HgX_4)$. This relationship is more likely to be followed in series of complexes with closely related ligands. The complexes $[Hg(S\text{-}2,4,6\text{-}^iPr_3C_6H_2)_2]$, $[Hg(S\text{-}2,4,6\text{-}^iPr_3C_6H_2)_3]^-$ and $[Hg(S\text{-}2\text{-}PhC_6H_4)_4]^{2-}$ ($\sigma_{iso}-\sigma_r = 1015$, 267 and 433 ppm respectively, Table 4) provide a good example of this.

In comparing shielding constants for complexes involving significantly different ligands, consideration must be given to the fact that these constants depend on the nature of the ligand through the Hg 6p orbital populations. This is true for the isotropic constant (Eq. (46)) as well as for the anisotropic constants (Eqs. (35)–(37)). For the linear HgX_2 case, Eq. (46) yields $\sigma_{iso} = (2/3)n_z\sigma_p$, compared with the corresponding expression for the shielding anisotropy $\Delta\sigma = -n_z\sigma_p$, so that a plot of $\Delta\sigma$ vs. $\sigma_{iso}-\sigma_r$ should be linear, with a slope of -1.5. Such a plot for a range of HgX_2 and HgXY compounds in Tables 3 and 4 is shown in Fig. 9. A reasonably linear relationship is indeed observed, but the slope is -2.2, somewhat more negative than the predicted value of -1.5. One possible reason for this more negative slope is the presence of secondary bonding. It was shown above that such interactions lead to a reduction in $\Delta\sigma$ (Eq. (44)), and a similar analysis using Eq. (46) shows that σ_{iso} should decrease as well. This would result in the displacement of points towards lower $\Delta\sigma$ and σ_{iso}. Since the degree of secondary bonding increases with decreasing σ-donor strength of the ligands X and Y involved in the primary X–Hg–Y bonding (see above), this effect would result in a more negative slope for the line in Fig. 9. However, it seems likely that differences in the details of the secondary bonding would lead to deviations from the linear relationship, and this may be the reason for systematic deviations which appear to occur for the X=SCN compounds and, to a lesser extent, for the X=CN compounds.

Another possible reason for the increased negative slope of the line in Fig. 9 is that there are contributions to σ_{iso} from terms other than the local paramagnetic ones. Thus, terms such as those arising from the Fermi-contact interaction, which are determined by electron density in the Hg 6s orbital, contribute equally to the anisotropic shielding parameters σ_{xx}, σ_{yy}, σ_{zz}, and so do not contribute at all to $\Delta\sigma$. The contribution of such terms to σ_{iso} should be proportional to the Hg 6s orbital population, which is expected to increase with the Hg 6p population. Thus, the additional shielding arising from such terms will be greater for $HgMe_2$ than for $HgCl_2$, for example, implying that the data in Fig. 9 are displaced to the right by this effect, and that the extent of this displacement decreases with increasing σ_{iso}. This would also explain the increase in the negative slope of this graph relative to that predicted by the model involving local paramagnetic terms only.

It is not possible at this stage to determine which of the above effects is more important in accounting for the observed deviation in the slope from the predicted

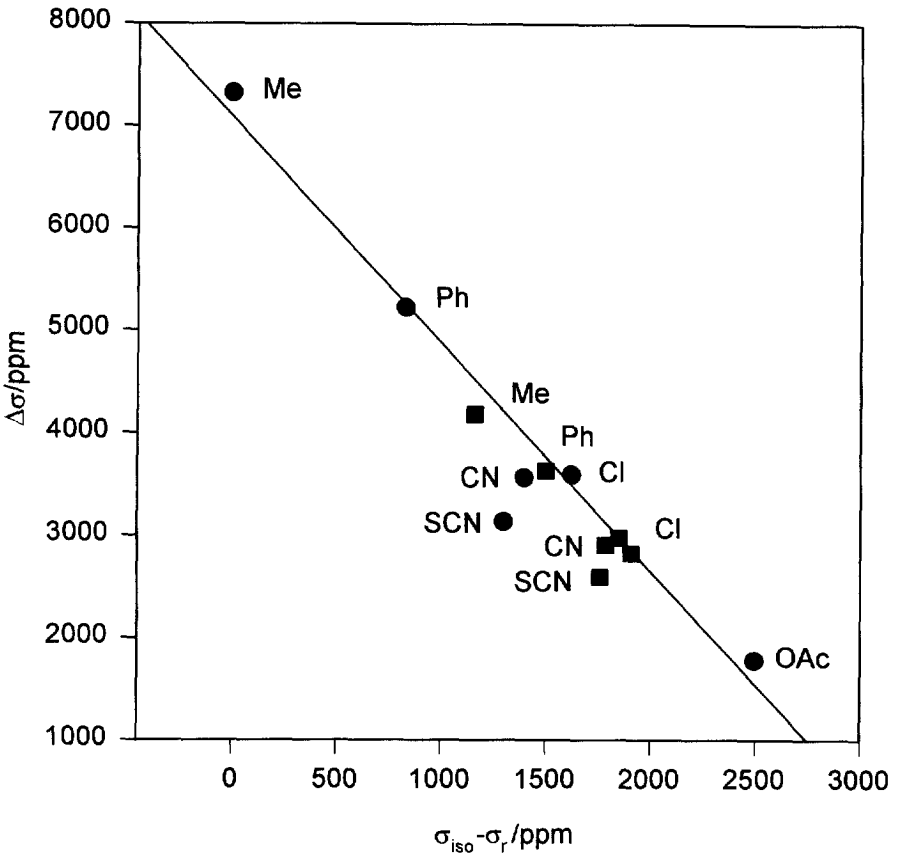

Fig. 9. Plot of the shielding anisotropy $\Delta\sigma$ for HgX_2 (●) and [Hg(X)OAc] (■) against the corresponding isotropic shielding constant $\sigma_{iso}-\sigma_r$.

value, or whether there is some other explanation, such as a breakdown of the average excitation energy approximation, or a variation in the average excitation energy from one complex to another. This can probably only be determined by theoretical calculations of the shielding parameters. However, the fact that the relationship in Fig. 9 corresponds reasonably well to the predictions based on consideration of local paramagnetic effects alone supports the view that such effects play a dominant role in the isotropic and anisotropic shielding.

Since the isotropic ^{199}Hg chemical shift can be easily and accurately measured in both solution- and solid-state spectra, and is sensitive to the Hg coordination environment, this parameter provides a means of detecting changes in structure between these two states. One example of this involves the complex $[Hg_2(SPh)_6]^{2-}$, which has a bridged dimeric structure with a distorted four-coordinate environment at the mercury atom in the solid state. There is a reduction in σ_{iso} from 560 ppm in the solid to 401 ppm in dimethylsulphoxide solution, and this has been attributed

to a dissociation of the dimer into $[Hg(SPh)_3]^-$ monomer species in solution [74]. A related example involves the compound $Hg(S^tBu)_2$ (infinite polymeric; four-coordinate Hg), which shows an increase in $\sigma_{iso}-\sigma_r$ from 665 ppm in the solid to 793 ppm in chloroform solution. This increase was attributed to a dissociation into a species involving linear HgS_2 coordination [10]. The complex $[Hg(SC_6H_4Cl)_4]^{2-}$ (four-coordinate Hg) shows an increase in $\sigma_{iso}-\sigma_r$ from 485 ppm in the solid to 569 ppm in dimethylsulphoxide solution. The presence of a dissociation reaction involving loss of thiolate ligand was demonstrated by the fact that the shielding decreases when excess thiolate is added to the solution [10]. The increase in σ_{iso} upon dissolution is somewhat surprising, as dissociation of one thiolate ligand would lead to the three-coordinate $[Hg(SC_6H_4Cl)_3]^-$ species, for which a reduction in shielding is expected. This result suggests that the dissociation proceeds further to give the neutral two-coordinate $[Hg(SC_6H_4Cl)_2]$ compound, and that the solution shielding constant is an average involving species with two-, three- and possibly four-coordinate mercury. The ^{199}Hg shielding constant measured for $[Hg(SOCPh)_3]^-$ in solution ($\sigma_{iso}-\sigma_r=750$ ppm) is much larger than that in $[Hg(SR)_3]^-$ ($\sigma_{iso}<350$ ppm in the solid state), even though both types of complex have planar HgS_3 skeletons in the solid state, and this was attributed to an interaction of the mercury atom with oxygen atoms in $[Hg(SOCPh)_3]^-$ [90]. However, this interaction is quite weak, judging by the long Hg–O distance observed in the crystal structure of the $[PPh_3]^+$ salt, and by analogy with the results discussed in the previous example above, it seems likely that the high shielding in solution is due to partial dissociation to two-coordinate $[Hg(SOCPh)_2]$. The above results illustrate how data obtained for well-characterized species in the solid state can be of use in interpreting solution-state NMR data.

4.3. Spin–spin coupling

Solid-state NMR studies of mercury compounds in which spin–spin coupling to mercury is observed appear to be restricted to the cases of coupling with ^{13}C, ^{31}P and ^{77}Se. Most investigations have dealt with the case of $^1J(HgP)$ coupling, and these will be considered first.

Single-crystal ^{31}P NMR studies have been reported for the compounds $Hg(PCy_3)(NO_3)_2$ [56] and $Hg(PPh_3)_2(NO_3)_2$ [57]. These have allowed the determination of the ^{199}Hg–^{31}P $\boldsymbol{J}$ tensor for the Hg–P bonds in these complexes. These spectra show an anisotropic splitting of the ^{199}Hg satellites, and the orientation-dependence of this splitting can be analyzed to yield the ^{199}Hg–^{31}P direct (dipolar) and indirect ($\boldsymbol{J}$) coupling tensors. The satellite line spacing $\Delta\nu$ is then given by

$$\Delta\nu = J - D'(3\cos^2\theta - 1) \tag{47}$$

where $\boldsymbol{D}'$ is the effective dipolar coupling constant $D'=D-\Delta J/3$, D is the ^{199}Hg–^{31}P dipolar coupling constant (Eq. (26)), and $\Delta J=J_{\parallel}-J_{\perp}$ is the anisotropy in $\boldsymbol{J}$. [Note that any asymmetry in $\boldsymbol{J}$ is generally ignored]. The isotropic, or scalar, coupling constant J is measured from the ^{31}P MAS spectrum of the complex, and

D is calculated from the Hg–P bond length (obtained from the X-ray crystal structure). This allows calculation of ΔJ and hence, from the isotropic coupling J, the principal components $J_{\parallel}$ and $J_{\perp}$ of J can be derived. The calculation requires knowledge of the sign of J, which has been shown to be positive [91]. The values of these parameters obtained for the two complexes mentioned above are given in Table 5, together with some earlier results obtained from ^{31}P NMR measurements on static powder samples [91–93]. It is clear from the data that the anisotropy in the indirect spin–spin coupling is substantial. This result indicates that indirect spin–spin coupling mechanisms in addition to the isotropic Fermi-contact mechanism are operative. There is some indication from the values in Table 5 that both J and ΔJ increase with increasing Hg–P bond strength (as indicated by Hg–P bond length or the electron-donating ability of the phosphorus donor ligand), but too few data are available to date to allow a more detailed correlation between ΔJ and the mercury coordination environment.

In principle, the J-anisotropy can also be investigated by sideband analysis of ^{199}Hg MAS NMR spectra of complexes which show ^{199}Hg–^{31}P coupling (Section 3.4). The necessary theory has been published for AX and linear AX_2 systems for the case where the σ and J tensors are axially symmetric and their principal axes lie along the relevant internuclear vector (and perpendicular to it) [76]. Very few ^{199}Hg MAS spectra have been reported which involve indirect spin–spin coupling to another $I=1/2$ nucleus, and none have yet been published for compounds with Hg–P or collinear P–Hg–P bonds in an axially symmetric environment. The only compound in Table 4 which involves coupling to ^{31}P is $[Hg(PCy_3)(OAc)_2]$; the ^{199}Hg CP MAS NMR spectrum of this complex consists of a centreband and spinning sidebands, all of which are split into doublets by the $^1J(^{199}Hg,^{31}P)$ coupling. The isotropic spin–spin coupling constant $J=8226$ Hz is readily obtained from the separation of the two centrebands, but no analysis for the anisotropic ^{199}Hg shielding tensor components was attempted [58]. The crystal structure of this complex shows that it exists as a doubly acetate-bridged dimer in the solid state, with a distorted tetrahedral O_3HgP coordination environment [94]. If this coordination arrangement had C_3 symmetry, then the condition of coincident

Table 5
^{199}Hg–^{31}P indirect spin–spin coupling tensor components (kHz) obtained from solid-state ^{31}P NMR experiments

Compound	J	$J_{\parallel}$	$J_{\perp}$	ΔJ	Ref.
$[Hg(PPh_3)(NO_3)_2]_2$	9.6	12.6	8.1	4.5	[91]
$[Hg(PCy_3)(NO_3)_2]_2$	8.0	11.7	6.2	5.5	[91]
$[Hg(PCy_3)(NO_3)_2]_\infty$	8.2	11.8	6.4	5.4	[56]
$[Hg(PPh_3)_2(NO_3)_2]$	5.5	8.2	4.2	4.0	[57]
$[Hg\{P(o\text{-}Tol)_3\}(NO_3)_2]_2$	9.66	13.11	7.94	5.17	[92]
$[Hg\{P(O)(OEt)_2\}(CH_3CO_2)]$	13.3	12.4	15.1	2.7	[93]
$[Hg\{P(O)(OEt)_2\}(SCN)]$	12.1	11.6	13.2	1.6	[93]
$[Hg\{P(O)(OEt)_2\}I]$	12.6	12.1	13.6	1.5	[93]

σ and J principal axes mentioned above would be met. Despite the lower symmetry in the present complex, near coincidence of these axes might be expected if the Hg–P bonding is stronger than the Hg–O bonding, causing near axial symmetry of the ^{199}Hg shielding tensor, the principal axis lying close to the Hg–P bond direction. This would manifest itself in a relatively large positive $\Delta\sigma$ and a small η value (see discussion in Section 4.1). Analysis of the spectrum by the previously published method (Section 3.4) [76] yields $\Delta\sigma = 2347$ ppm, $\eta = 0.16$ and $\Delta J = 5.1$ kHz. The expectations discussed above concerning $\Delta\sigma$ and η are thus met; the values of these parameters are in fact very similar to those for [Hg(RS)L] (R = Me, Et; L = tris(3,5-dimethylpyrazol-1-yl)hydroborate; Table 4) which have an N_3HgS coordination environment in which the Hg–S bonding is dominant (Section 4.1). This lends support to the hypothesis of strong Hg–P bonding and the dominant influence of this bonding on the ^{199}Hg σ tensor in the present complex. The ΔJ value is quite similar to those obtained from ^{31}P NMR spectra of related complexes (Table 5), demonstrating that such information is obtainable from spinning sideband analysis of ^{199}Hg spectra as well as from ^{31}P NMR spectra. However, the accuracy of the analysis depends heavily on the quality of the spectra.

Solid-state ^{31}P NMR spectra have been reported for a range of mercury(II) complexes with phosphine ligands. The results of these studies are summarized in Table 6, and these demonstrate how such spectra can yield information on the structure of complexes in the solid state. This is well illustrated by the ^{31}P CP MAS results for 1:1 and 2:1 complexes of phosphine ligands with mercury (II) halides [95,96]. The 2:1 complexes all have mononuclear $[L_2HgX_2]$ structures. However, the NMR spectra clearly distinguish between the cases in which the two phosphines ligands are crystallographically equivalent and those in which they are not equivalent in the solid. In the case where they are equivalent, the ^{199}Hg satellites simply consist of a doublet which is the A part of an A_2X spin system, e.g. $[Hg(PEt_3)_2Cl_2]$ (Table 6). When the two ligands are not crystallographically equivalent, an ABX pattern is observed, e.g. $[Hg(PEt_3)_2Br_2]$ (Table 6). In such cases, the inequivalence of the two phosphorus atoms allows the observation of ^2J(PP) coupling as well as ^1J(HgP) coupling. There are a number of different possible structures for the 1:1 complexes. One is the dimeric, doubly halogen-bridged structure $[L(X)Hg(\mu\text{-}X)_2HgL(X)]$, and the NMR spectra allow a distinction to be made between centrosymmetric and non-centrosymmetric forms of this structure. In the centrosymmetric form, the two Hg–P bonds are equivalent, and the ^{199}Hg satellites consist of a simple doublet which is the A part of two equivalent AX spin systems, which display no magnetic interaction with each other (the coupling via the halogen bridges is negligible), e.g. $[Hg_2(PPh_3)_2Cl_4]$ (Table 6). In the non-centrosymmetric case, two doublets are observed, as the two Hg–P bonds are no longer equivalent, e.g. $[Hg_2(PPh_3)_2Br_4]$ (Table 6). A different kind of dimeric structure is the lower symmetry $[L_2Hg(\mu\text{-}X)_2HgX_2]$ arrangement. This also gives rise to an ABX pattern, e.g. $[Hg_2(PBu_3)_2I_4]$ (Table 6). In this case the spectrum is further complicated by the presence of two crystallographically inequivalent dimers in the asymmetric unit, so that two ABX patterns are observed. These observations allow the determination of structural information for complexes whose crystal structures have not been

Table 6
Solid-state ^{31}P NMR parameters for some mercury(II) complexes with phosphine ligands

Complex[a]	Spin system[b]	$\delta(^{31}P)$ (ppm)		$\lvert^1J(^{199}HgP)\rvert$ (Hz)		$\lvert^2J(PP)\rvert$ (Hz)	Ref.
		δ_A	δ_B	J_{AX}	J_{BX}	J_{AB}	
$[Hg(PPh_3)(NO_3)_2]_2$	AX	32.2	–	9572	–	–	[91]
$[Hg(PCy_3)(NO_3)_2]_2$	AX	79.5	–	8008	–	–	[91]
$[Hg(PCy_3)(NO_3)_2]_\infty$	AX	71	–	8199	–	–	[56]
	AX	72	–	8199	–	–	
$[Hg(PPh_3)_2(NO_3)_2]$	A_2X[c]	40	–	5550	–	250[d]	[57]
$[Hg(PPh_3)Cl](NO_3)$	AX	30.5	–	8085	–	–	[53]
$[Hg(PPh_3)Br](NO_3)$	AX	32.2	–	7400	–	–	[53]
$[Hg(PPh_3)I](NO_3)$	AX	33.0	–	6330	–	–	[53]
$[Hg_2(PPh_3)_2Cl_4]$	AX	39.6	–	7448	–	–	[95]
$[Hg_2(PPh_3)_2Br_4]$	AX	33.8	–	6264	–	–	[95]
	AX	35.4	–	6611	–	–	
$[Hg_2(PPh_3)_2I_4]$	AX	11.9	–	4428	–	–	[95]
	AX	14.8	–	4957	–	–	
$[Hg(PPh_3)_2Cl_2]$	ABX	~27	~27	~4600	~4600	180	[95]
$[Hg(PPh_3)_2Br_2]$	ABX	13.0	18.5	4182	3183	164	[95]
$[Hg(PPh_3)_2I_2]$	ABX	2.0	6.8	2644	2330	154	[95]
$[Hg_2(PEt_3)_2Cl_4]$[e]	AX	46.9	–	7928	–	–	[95]
$[Hg_2(PEt_3)_2Br_4]$[e]	AX	38.8	–	7028	–	–	[95]
$[Hg_2(PEt_3)_2I_4]$[e]	AX	21.5	–	5268	–	–	[95]
$[Hg(PEt_3)_2Cl_2]$	A_2X	44.9	–	5287	–	–	[95]
$[Hg(PEt_3)_2Br_2]$	ABX	32.9	34.7	4579	4445	166	[95]
$[Hg(PEt_3)_2I_2]$	ABX	20.4	21.5	4007	4141	120	[95]
$[Hg_2(PBu_3)_2Cl_4]$	AX	37.2	–	7285	–	–	[95]
	AX	38.2	–	7344	–	–	
$[Hg_2(PBu_3)_2Br_4]$	ABX	34.4	37.0	5111	5175	173	[95]
	ABX	36.3	38.3	4833	4911	182	
$[Hg_2(PBu_3)_2I_4]$	ABX	19.4	23.7	5032	5102	147	[95]
	ABX	22.2	25.3	4691	4793	158	
$[Hg(PBu_3)_2Cl_2]$	ABX	30.1	35.1	4621	4826	170	[95]

[a] Ligand abbreviations: PBu_3 = tri-*n*-butylphosphine. [b] A,B = ^{31}P; X = ^{199}Hg.
[c] Single-crystal spectrum shows ABX or AMX character, depending on orientation of the crystal in the magnetic field.
[d] From variable-angle spinning (VAS) or slow MAS spectra ([90,91]).
[e] The dimer units are loosely associated to form an infinite chain structure.

determined. Thus, for example, $[Hg_2(PBu_3)_2Br_4]$ (Table 6) must have the lower symmetry $[L_2Hg(\mu\text{-}X)_2HgX_2]$ structure observed in the iodide, rather than the higher symmetry $[L(X)Hg(\mu\text{-}X)_2HgL(X)]$ structure observed in the chloride.

Examples of polymorphism are also readily detected by the ^{31}P MAS NMR spectra. Thus, two forms of the 1:1 adduct of PCy_3 with $Hg(NO_3)_2$ (a dimeric and an infinite polymeric form) give significantly different $^1J(^{199}HgP)$ values (Table 6) [56,91]. In the case of $[Hg_2(DMPP)_2I_4]$ (DMPP = 3,4-dimethylphosphole), the observation of three AX patterns indicates the presence of a phase with a centrosymmetric structure (single AX pattern) as well as the non-centrosymmetric phase (two AX patterns) observed in a crystal structure determination [95].

In addition to the satellites which yield the $^{1}J(^{199}HgP)$ coupling constants listed in Table 6, the ^{31}P CP MAS NMR spectra of $[Hg(PPh_3)X]NO_3$ (X=Cl, Br, I) also show broader satellites which have been attributed to $^{1}J(^{201}HgP)$ coupling [53]. The spectrum of the iodide is shown in Fig. 10. These compounds display essentially linear P–Hg–X coordination, for which large ^{201}Hg quadrupole coupling constants ($|\chi| \approx 700$ MHz) are expected (Section 2.4). The splitting patterns in the MAS NMR spectra of an $I=1/2$ nucleus coupled to an $I>1/2$ nucleus have been discussed by a number of authors [97–102]. Menger and Veeman have reported calculations of the line positions in the spectrum of an $I=1/2$ nucleus coupled to an $I=3/2$ nucleus in terms of the various coupling constants involved [97]. For the case where the spin $I=1/2$ nucleus is ^{31}P and the quadrupolar nucleus is a metal atom M, the relevant parameters are the metal nuclear Zeeman interaction $Z=\gamma_M hB$, the metal nuclear quadrupole coupling constant $\chi=e^2qQ/h$, the phosphorus–metal dipolar coupling

Fig. 10. 121.5 MHz ^{31}P CP MAS NMR spectrum of $[Hg(PPh_3)I]NO_3$; × = impurity; the peaks assigned as ^{201}Hg satellites are arrowed. The vertical scale of the upper trace is expanded (ca. ×4) relative to that of the lower trace [reproduced, with permission, from Ref. [53]].

constant $D=(\mu_0/4\pi)(\gamma_P\gamma_M/r^3)(\hbar/2\pi)$ (r = the M–P bond length) and the indirect spin–spin coupling constant J. The form of the spectrum depends on the ratio $R=D/J$ of the dipolar to the indirect coupling constant and on the dimensionless parameter

$$K=-3\chi/4I(2I-1)Z \tag{48}$$

which is proportional to the ratio of the metal quadrupole coupling constant to the metal nuclear Zeeman term. The analysis has been presented for three cases; where the spin 1/2-spin 3/2 interaction is purely dipolar, where it is purely scalar, and where mixed dipolar/scalar interactions exist [97]. The last-mentioned case occurs in the ^{31}P CP MAS NMR spectra of compounds containing Cu–P bonds, where asymmetric quartets are normally observed due to coupling of ^{31}P to the quadrupolar $^{63,65}Cu$ nuclei ($I=3/2$). In this case R lies in the range 0.5 to 1.0 and K lies in the range 0 to 0.5 so the observed spectra consist of asymmetric quartets [97]. For $[Hg(PPh_3)X]^+$ R is much smaller than for the $^{63,65}Cu/^{31}P$ case, and the situation corresponds more closely to the purely scalar coupling case for which a symmetric quartet, with line spacings equal to J, is predicted for the case $K\approx 0$ (corresponding to cubic symmetry at the Hg atom). For complexes involving linear two-coordinate Hg, however, the quadrupole coupling constant is expected to be much larger. For a ^{201}Hg quadrupole coupling constant $|\chi|=700$ MHz, and a ^{201}Hg Zeeman interaction $Z=19.8$ MHz ($B=7.05$ T), $K\approx 9$, Eq. (48). It has been shown that for $K>10$ the spectrum should consist of two lines with a spacing of about $1.65J$ [53,54]. Since $^1J(^{201}HgP)/^1J(^{199}HgP)=\gamma(^{201}Hg)/\gamma(^{199}Hg)=0.369$, the spacing of the ^{201}Hg satellites should be $1.65\times 0.396\ ^1J(^{199}HgP)=0.61\ ^1J(^{199}HgP)$, which agrees well with the observed spacing of the pair of lines assigned as the ^{201}Hg satellites, shown in Fig. 10. The compounds $[Hg(PPh_3)X]NO_3$ remain the only ones to date for which scalar coupling to ^{201}Hg has been observed, although doublet splittings in $[Au(PPh_3)X]$ (isoelectronic with $[Hg(PPh_3)X]^+$) and $[Au(PMe_3)X]$ which have been attributed to $^1J(^{197}AuP)$ coupling have also been reported [103,104]. A theoretical treatment of quadrupole effects on MAS NMR spectra of $I=1/2$ nuclei in the limit of large quadrupole coupling constants has been presented, and the line positions and powder lineshapes for coupling to an $I=3/2$ nucleus with parameters similar to those observed for $[(PPh_3)HgX]NO_3$ have been calculated [54]. These agree well with the experimental observations for these compounds.

There have been relatively few reports of the observation of scalar coupling between ^{199}Hg and ^{13}C in the solid state. The data are summarized in Table 7. The $^1J(^{199}Hg^{13}C)$ values observed for organomercury compounds are similar to those reported for the same compounds in solution [105,106]. In these reports, comment is made on the uncertainty of the role of ^{201}Hg in the spectra, since the ratio of the centreband intensity (due to non-magnetic isotopes of mercury) to the ^{199}Hg satellite intensities is sometimes less than expected. The more recent results on the role of ^{201}Hg in the ^{31}P MAS NMR spectra of compounds with Hg–P bonds (see above) may be relevant in this connection.

Perhaps the most remarkable result in Table 7 is the very large value of $^1J(^{199}Hg^{13}C)$ in $[Hg(CO)_2]^{2+}$ which is unprecedented in organomercury chemistry

Table 7
Solid-state ^{13}C NMR parameters for some mercury complexes

Complex	$\delta(^{13}C)$ (ppm)	$\lvert^1J(^{199}Hg–^{13}C)\rvert$ (Hz)	$\lvert^nJ(^{199}Hg–^{13}C)\rvert$ (Hz)	Ref.
$Hg(CF_3)_2$	–	2820	–	[105]
$Hg(CH_3)Cl$	8.31	1807	–	[106]
$Hg(CH_3)OAc$	0.09	1847	–	[106]
$Hg(CH_3)S_2COCH_3$	9.07	1445	–	[106]
$K_2[Hg(CN)_4]$	153.1	1540	–	[52]
$Hg(CN)_2$	149.5	3315	–	[82]
$[Hg(CO)_2][Sb_2F_{11}]_2$	168.8	5219	–	[107]
$[Hg_2(CO)_2][Sb_2F_{11}]_2$	188.7	3350	850 (^2J)	[107]
$Hg(OAc)_2$	180.9	–	118 (^2J)	[108]
	176.8	–	156 (^2J)	
	24.7	–	176 (^3J)	
	24.3	–	195 (^3J)	
Hg(SCN)OAc	180.6	–	119 (^2J, OAc)	[82]
	23.3	–	143 (^3J, OAc)	

[107]. This coupling could not be observed in solution, presumably due to ligand exchange processes [107]. This illustrates the value of high-resolution solid-state NMR in providing data for unusual and highly reactive species.

The ^{13}C CP MAS NMR spectrum of mercury(II) acetate, $Hg(OAc)_2$, shows the inequivalence of the two acetate groups [108], which was subsequently verified by an X-ray structure determination [109]. The spectrum also shows $^2J(^{199}Hg^{13}C)$ satellites on the carbonyl carbon signals, and $^3J(^{199}Hg^{13}C)$ satellites on the methyl carbon signals. This coupling is not evident in the solution-state spectrum, despite the narrower lines, because of the occurrence of ligand exchange processes in solution [108]. Similar long-range couplings have subsequently been seen in other mercury complexes involving an acetate ligand [82], but not in all such complexes which have been studied [82,106]. It appears that such couplings are at the limit of the resolution currently available in solid-state MAS NMR spectra.

Two studies of compounds with Hg–Se bonds by ^{77}Se MAS NMR spectroscopy have been reported [83,110]. In $Hg(SeCN)_2$, $\lvert^1J(^{199}Hg^{77}Se)\rvert = 965$ Hz. It would be difficult to measure this quantity in solution, due to the low solubility of this compound, and its instability in solution. While the $^1J(^{199}Hg^{77}Se)$ coupling is clearly resolved in the ^{77}Se MAS NMR spectrum, it is not visible at all in the corresponding ^{199}Hg spectrum, because of the greater linewidths in this spectrum [83]. In $[Me_4N]_2[Hg(Se_4)_2]$, in which the Hg atom is tetrahedrally coordinated by two chelating tetraselenide (Se_4^{2-}) ligands, separate signals with associated spinning sideband manifolds are seen for all eight Se atoms! ^{199}Hg satellites are resolved on all but one of these signals, yielding $\lvert^1J(^{199}Hg^{77}Se)\rvert = 1220$–$1480$ Hz and $\lvert^2J(^{199}Hg^{77}Se)\rvert \approx 330$ Hz [110]. This can be compared with the solution-state spectrum, in which there are only two signals: metal-bound ($\lvert^1J(^{199}Hg^{77}Se)\rvert = 1265$ Hz) and ring (no ^{199}Hg satellites reported) [111].

5. Conclusion

Five years ago a review of the applications of solid-state NMR spectroscopy of metal nuclei in organometallic and coordination chemistry quoted only three references on mercury compounds [15]. The present review shows the greatly increased activity which has occurred in the last five years, and demonstrates that more quantitative interpretations of the data are now possible. Although this review is restricted to mercury compounds, the methods and principles involved are of wider applicability in the analysis of solid-state NMR spectroscopy of metal complexes, and it is expected that further developments will continue to enhance the utility of this area of spectroscopy in coordination chemistry.

References

[1] R.K. Harris, B.E. Mann (Eds.), NMR and the Periodic Table, Academic Press, London, 1978.
[2] P. Laszlo (Ed.), NMR of Newly Accessible Nuclei, Academic Press, New York, 1983.
[3] B. Wrackmeyer, in: G.A. Webb (Ed.), Annu. Rep. NMR Spectrosc., vol. 16, Academic Press, New York, 1985, p. 73.
[4] P.S. Pregosin, in: G.A. Webb (Ed.), Annu. Rep. NMR Spectrosc., vol. 17, Academic Press, New York, 1986, p. 285.
[5] R.J. Goodfellow, in: J. Mason (Ed.), Multinuclear NMR, Plenum, London, 1987, p. 563.
[6] B. Wrackmeyer, K. Horchler, in: G.A. Webb (Ed.), Annu. Rep. NMR Spectrosc., vol. 22, Academic Press, New York, 1989, p. 249.
[7] B.E. Mann, in: G.A. Webb (Ed.), Annu. Rep. NMR Spectrosc., vol. 23, Academic Press, New York, 1991, p. 141.
[8] P. Granger, in: P.S. Pregosin (Ed.), Studies in Inorganic Chemistry 13. Transition Metal Nuclear Magnetic Resonance, Elsevier, Amsterdam, 1991, p. 264.
[9] B. Wrackmeyer, R. Contreras, in: G.A. Webb (Ed.), Annu. Rep. NMR Spectrosc., vol. 24, Academic Press, New York, 1992, p. 267.
[10] J.G. Wright, M.J. Natan, F.M. MacDonnell, D.M. Ralston, T.V. O'Halloran, Prog. Inorg. Chem. 38 (1990) 323.
[11] M.F. Summers, Coord. Chem. Rev. 86 (1988) 43.
[12] U. Haeberlen, Adv. Magn. Reson., Suppl. 1 (1976).
[13] C.A. Fyfe, Solid State NMR for Chemists, CFC Press, Guelph, 1983.
[14] R.K. Harris, Nuclear Magnetic Resonance Spectroscopy, Longman, Harlow, 1986.
[15] J.A. Davies, S. Dutremez, Coord. Chem. Rev. 114 (1992) 201.
[16] A. Sebald, NMR Basic Principles and Progress 31 (1994) 91.
[17] R.K. Harris, P. Jackson, L.H. Merwin, B.J. Say, J. Chem. Soc. Faraday Trans. 1 84 (1988) 3649.
[18] R.K. Harris, Chem. Britain (1993) 601.
[19] M. Mehring, in: P. Diehl, E. Fluck, H. Günther, R. Kosfeld (Eds.), NMR Basic Principles and Progress, vol. 11, Springer Verlag, Berlin, 1976.
[20] P. Diehl, E. Fluck, H. Günther, R. Kosfeld, J. Seelig (Eds.), NMR Basic Principles and Progress, vols. 30–33, Springer Verlag, Berlin, 1994.
[21] E.O. Stejskal, J.D. Memory, High Resolution NMR in the Solid State, Oxford University Press, Oxford, 1994.
[22] R.K. Harris, Nuclear spin properties and notation, in: D.M. Grant, R.K. Harris (Eds.), Encyclopedia of Nuclear Magnetic Resonance, vol. 5, Wiley, Chichester, 1996, p. 3301.
[23] J.G. Verkade, J.A. Mosbo, in: J.G. Verkade, L.D. Quin (Eds.), Phosphorus-31 N.M.R. Spectroscopy in Stereochemical Analysis, VCH Publishers, Deerfield Beach, Fl, 1987, pp. 425–463.

[24] P.S Pregosin, ^{31}P and ^{13}C NMR of Transition Metal Phosphine Complexes, NMR Basic Principles and Progress, P. Diehl, E. Fluck, R. Kosfeld (Eds.), Vol. 16, Springer-Verlag, Berlin, 1979.
[25] M. Delnomdedieu, D. Georgescauld, A. Boudou, E.J. Dufourc, Bull. Magn. Reson. 11 (1989) 420.
[26] K. Brodersen, H.-U. Hummel, in: G. Wilkinson (Ed.), Comprehensive Coordination Chemistry, vol. 5, Pergamon, Oxford, 1987, p. 1047.
[27] W. Levason, C.A. McAuliffe, The coordination chemistry of mercury, in: C.A. McAuliffe (Ed.), The Chemistry of Mercury, McMillan, London, 1977.
[28] A.J. Canty, G.B. Deacon, Inorg. Chim. Acta 45 (1980) L225.
[29] A.F. Wells, Structural Inorganic Chemistry, 5th ed., Clarendon Press, Oxford, 1984, pp. 1156–1169.
[30] D. Grdenic, Q. Rev. Chem. Soc. 19 (1965) 303.
[31] P.A.W. Dean, Prog. Inorg. Chem. 24 (1978) 109.
[32] G.A. Bowmaker, Adv. Spectrosc. 14 (1987) 1.
[33] J. Mason, Solid state NMR 2 (1993) 285.
[34] G.E. Hawkes, K.D. Sales, L.Y. Lian, R. Gobetto, Proc. R. Soc., Lond., Part A 424 (1989) 93.
[35] Pure Appl. Chem. 29 (1972) 627; 45 (1976) 217.
[36] C.J. Groombridge, Magn. Reson. Chem. 31 (1993) 380.
[37] J.M. Hook, P.A.W. Dean, L.C.M. van Gorkom, Magn. Reson. Chem. 33 (1995) 77.
[38] J.M. Hook, P.A.W. Dean, D.C.R. Hockless, Acta Cryst., Part C 51 (1995) 1547.
[39] G.A. Webb, Factors contributing to the observed chemical shifts of heavy nuclei, in: P. Laszlo (Ed.), NMR of Newly Accessible Nuclei, vol. 1, Academic Press, New York, 1983, p. 79.
[40] N.F. Ramsey, Phys. Rev. 78 (1950) 689.
[41] J.A. Pople, J. Chem. Phys. 37 (1962) 53; 37 (1962) 60; Mol. Phys. 7 (1964) 301.
[42] C.J. Jameson, H.S. Gutowsky, J. Chem. Phys. 40 (1964) 1714.
[43] M. Karplus, T.P. Das, J. Chem. Phys. 34 (1961) 1683.
[44] H. Nakatsuji, M. Hada, H. Kaneko, C.C. Ballard, Chem. Phys. Lett. 255 (1996) 195.
[45] N.F. Ramsey, Phys. Rev. 91 (1953) 303.
[46] C.J. Jameson, in: J. Mason (Ed.), Multinuclear NMR, Plenum Press, New York, 1987, pp. 89–131.
[47] C.J. Jameson, in: J.G. Verkade, L.D. Quin (Eds.), Phosphorus-31 N.M.R. Spectroscopy in Stereochemical Analysis, VCH Publishers, Deerfield Beach, Fl, 1987, pp. 205–230.
[48] E.A.C. Lucken, Nuclear Quadrupole Coupling Constants, Academic Press, London, 1969.
[49] D.B. Patterson, G.E. Peterson, A. Carnevale, Inorg. Chem. 12 (1973) 1283.
[50] G.A. Bowmaker, P.D.W. Boyd, R.J. Sorrenson, J. Chem. Soc. Faraday Trans. I 81 (1985) 1627.
[51] G. Wu, R.E. Wasylishen, Magn. Reson. Chem. 31 (1993) 537.
[52] G. Wu, S. Kroeker, R.E. Wasylishen, Inorg. Chem. 34 (1995) 1595.
[53] L.-J. Baker, G.A. Bowmaker, P.C. Healy, B.W. Skelton, A.H. White, J. Chem. Soc. Dalton Trans. (1992) 989.
[54] A.C. Olivieri, Solid State Nucl. Magn. Reson. 1 (1992) 345.
[55] R.A. Santos, G.S. Harbison, J. Am. Chem. Soc. 116 (1994) 3075.
[56] M.D. Lumsden, K. Eichele, R.E. Wasylishen, T.S. Cameron, J.F. Britten, J. Am. Chem. Soc. 116 (1994) 11129.
[57] M.D. Lumsden, R.E. Wasylishen, J.F. Britten, J. Phys. Chem. 99 (1995) 16602.
[58] F. Ambrosius, E. Klaus, T. Schaller, A. Sebald, Z. Naturforsch., Teil A 50 (1995) 423.
[59] R.K. Harris, A. Sebald, Magn. Reson. Chem. 25 (1987) 1058.
[60] R.A. Santos, E.S. Gruff, S.A. Koch, G.S. Harbison, J. Am. Chem. Soc. 113 (1991) 469.
[61] E.O. Stejskal, J. Schaefer, J.S. Waugh, J. Magn. Reson. 28 (1977) 105.
[62] O.B. Peersen, X. Wu, I. Kustanovich, S.O. Smith, J. Magn. Reson. Ser. A 104 (1993) 334.
[63] G. Metz, X. Wu, S.O. Smith, J. Magn. Reson. Ser. A 110 (1994) 219.
[64] M. Han, O.B. Peersen, J.W. Bryson, T.V. O'Halloran, S.O. Smith, Inorg. Chem. 34 (1995) 1187.
[65] M.M. Maricq, J.S. Waugh, J. Chem. Phys. 70 (1979) 3300.
[66] J. Herzfeld, A.E. Berger, J. Chem. Phys. 73 (1980) 6021.
[67] N.J. Clayden, C.M. Dobson, L.-Y. Lian, D.J. Smith, J. Magn. Reson. 69 (1986) 476.
[68] B.Q. Sun, A. Pines, Appl. Magn. Reson. 5 (1993) 43.
[69] D. Fenzke, B. Maess, H. Pfeifer, J. Magn. Reson. 88 (1990) 172.

[70] L.H. Merwin, Ph.D. thesis, University of Durham, 1987;
H.-P. Bai, Ph.D. thesis, University of Durham, 1991.
[71] R.K. Harris, L.H. Merwin, G. Hägele, J. Chem. Soc. Faraday Trans. I (1989) 1409.
[72] H.J.M. deGroot, S.O. Smith, A.C. Kolbert, J.M.L. Courtin, C. Winkel, J. Lugtenburg, J. Herzfeld, R.G. Griffin, J. Magn. Reson. 91 (1991) 30.
[73] J. Herzfeld, X. Chen, Sideband analysis in magic angle spinning NMR of solids, in: D.M. Grant, R.K. Harris (Eds.), Encyclopedia of Nuclear Magnetic Resonance, vol. 9, Wiley, Chichester, 1996, p. 4362.
[74] G.A. Bowmaker, I.G. Dance, R.K. Harris, W. Henderson, I. Laban, M. Scudder, Se-Woung Oh, J. Chem. Soc. Dalton Trans. (1996) 2381.
[75] G. Jeschke, G. Grossmann, J. Magn. Reson. Ser. A 103 (1993) 323.
[76] H. Bai, R.K. Harris, J. Magn. Reson. 96 (1992) 24.
[77] A.C. Olivieri, J. Magn. Reson. Ser. A 123 (1996) 207.
[78] J.D. Kennedy, W. McFarlane, J. Chem. Soc. Faraday Trans. II 72 (1976) 1653.
[79] J. Jokisaari, P. Diehl, Org. Magn. Reson. 13 (1980) 359.
[80] R.E. Wasylishen, R.E. Lenkinski, C. Rodger, Can. J. Chem. 60 (1982) 2113.
[81] Y.K. Grishin, D.V. Bazhenov, Y.A. Ustynyuk, V.M. Mastikhin, Zh. Strukt. Khim. 28 (1987) 45; J. Struct. Chem. 28 (1987) 850.
[82] G.A. Bowmaker, A.V. Churakov, R.K. Harris, Se-Woung Oh, J. Organomet. Chem., in press.
[83] G.A. Bowmaker, A.V. Churakov, R.K. Harris, J.A.K. Howard, D.C. Apperley, Inorg. Chem., in press.
[84] M.J. Natan, C.F. Millikan, J.G. Wright, T.V. O'Halloran, J. Am. Chem. Soc. 112 (1990) 3255.
[85] K. Eichele, S. Kroeker, G. Wu, R.E. Wasylishen, Solid State NMR 4 (1995) 295.
[86] R.K. Harris, Se-Woung Oh, unpublished results.
[87] G. Wu, R.E. Wasylishen, J. Phys. Chem. 97 (1993) 7863.
[88] S. Aime, G. Digilio, R. Gobetto, P. Cecchi, G. Gioia-Lobbia, M. Camalli, Polyhedron 13 (1994) 2695.
[89] A. Iverfeldt, I. Persson, Inorg. Chim. Acta 111 (1986) 171.
[90] J.J. Vittal, P.A.W. Dean, Inorg. Chem. 35 (1996) 3089.
[91] W.P. Power, M.D. Lumsden, R.E. Wasylishen, J. Am. Chem. Soc. 113 (1991) 8257.
[92] G.H. Penner, W.P. Power, R.E. Wasylishen, Can. J. Chem. 66 (1988) 1821.
[93] W.P. Power, M.D. Lumsden, R.E. Wasylishen, Inorg. Chem. 30 (1991) 2997.
[94] E.C. Alyea, S.A. Dias, G. Ferguson, M.A. Khan, P.J. Roberts, Inorg. Chem. 18 (1979) 2433.
[95] G.A. Bowmaker, H.J. Clase, N.W. Alcock, J.M. Kessler, J.H. Nelson, J.S. Frye, Inorg. Chim. Acta 210 (1993) 107.
[96] T. Allman, R.E. Lenkinski, Inorg. Chem. 25 (1986) 3202.
[97] E.M. Menger, W.S. Veeman, J. Magn. Reson. 46 (1982) 257.
[98] R.K. Harris, J. Magn. Reson. 78 (1988) 389.
[99] A.C. Olivieri, J. Magn. Reson. 81 (1989) 201.
[100] A. Olivieri, J. Am. Chem. Soc. 114 (1992) 5758.
[101] R.K. Harris, A.C. Olivieri, Prog. Nucl. Magn. Reson. Spectrosc. 24 (1992) 435.
[102] A.C. Olivieri, J. Magn. Reson. Ser. A 101 (1993) 313.
[103] P.F. Barron, L.M. Engelhardt, P.C. Healy, J. Oddy, A.H. White, Aust. J. Chem. 40 (1987) 1545.
[104] K. Angermair, G.A. Bowmaker, E.N. de Silva, P.C. Healy, B.E. Jones, H. Schmidbaur, J. Chem. Soc. Dalton Trans. (1996) 3121.
[105] R.D. Kenrick, C.S. Yannoni, R. Aikman, R.G. Lagow, J. Magn. Reson. 37 (1980) 555.
[106] A.M. Hounslow, S.F. Lincoln, E.R.T. Tiekink, J. Organomet. Chem. 354 (1988) C9.
[107] M. Bodenbinder, G. Balzer-Jöllenbeck, H. Willner, R.J. Batchelor, F.W.B. Einstein, C. Wang, F. Aubke, Inorg. Chem. 35 (1996) 82;
H. Willner, M. Bodenbinder, C. Wang, F. Aubke, J. Chem. Soc. Chem. Comm. (1994) 1189.
[108] P.F. Barron, J. Organomet. Chem. 236 (1982) 157.
[109] R. Allmann, Z. Kristallogr. 138 (1973) 366.
[110] P.J. Barrie, R.J.H. Clark, R. Withnall, D.-Y. Chung, K.-W. Kim, M.G. Kanatzidis, Inorg. Chem. 33 (1994) 1212.
[111] M.A. Ansari, C.H. Mahler, G.S. Chorghade, Y.-J. Lu, J.A. Ibers, Inorg. Chem. 29 (1990) 3832.